

A high-resolution spectroscopic survey of late-type stars: chromospheric activity, rotation, kinematics, and age^{★,★★}

J. López-Santiago¹, D. Montes¹, M. C. Gálvez-Ortiz², I. Crespo-Chacón¹, R. M. Martínez-Arnáiz¹,
M. J. Fernández-Figueroa¹, E. de Castro¹, and M. Cornide¹

¹ Departamento de Astrofísica y Ciencias de la Atmósfera, Universidad Complutense de Madrid, 28040 Madrid, Spain
e-mail: jls@astrax.fis.ucm.es

² Centre For Astrophysics Research, University of Hertfordshire, College Lane, Hatfield, Hertfordshire, AL10 9AB, UK

Received 9 October 2009 / Accepted 5 February 2010

ABSTRACT

Aims. We present a compilation of spectroscopic data from a survey of 144 chromospherically active young stars in the solar neighborhood, which may be used to investigate different aspects of its formation and evolution in terms of kinematics and stellar formation history. The data have already been used by us in several studies. With this paper, we make all these data accessible to the scientific community for future studies on different topics.

Methods. We performed spectroscopic observations with *echelle* spectrographs to cover the entirety of the optical spectral range simultaneously. Standard data reduction was performed with the IRAF ECHELLE package. We applied the spectral subtraction technique to reveal chromospheric emission in the stars of the sample. The equivalent width of chromospheric emission lines was measured in the subtracted spectra and then converted to fluxes using equivalent width-flux relationships. Radial and rotational velocities were determined by the cross-correlation technique. Kinematics, equivalent widths of the lithium line $\lambda 6707.8$ Å and spectral types were also determined.

Results. A catalog of spectroscopic data is compiled: radial and rotational velocities, space motion, equivalent widths of optical chromospheric activity indicators from Ca II H & K to the calcium infrared triplet and the lithium line in $\lambda 6708$ Å. Fluxes in the chromospheric emission lines and R'_{HK} are also determined for each observation of a star in the sample. We used these data to investigate the emission levels of our stars. The study of the H α emission line revealed two different populations of chromospheric emitters in the sample, clearly separated in the $\log F_{H\alpha}/F_{bol} - (V - J)$ diagram. The dichotomy may be associated with the age of the stars.

Key words. Galaxy: stellar content – solar neighborhood – stars: late-type – stars: activity – stars: chromospheres

1. Introduction

The velocity (or phase) space in the solar neighborhood is rather complicated. In particular, the *UV*-plane shows different structures that are associated with the Galactic potential characteristics. At large scales, the *UV*-plane is dominated by long branches (Skuljan et al. 1999) related to dynamical perturbations altering the kinematics of the solar neighborhood (Famaey et al. 2005), including the resonance of the rotating bar (Famaey et al. 2007; Antoja et al. 2009). The fine structure of the velocity distribution of disk stars is more likely related to the existence of the classic Eggen moving groups (see Montes et al. 2001a, for a review of the young moving groups problem). In fact, the substructures found inside the long branches appear to have on average different ages (Asiain et al. 1999; Antoja et al. 2008), which agree with the idea of the moving groups being formed by coeval stars. These young substructures are mixed in phase space with old stars and it is difficult to discern between young and old stars only by their kinematics. In some cases, the vertical component of the Galactic velocity (*W*) can be used to reject membership of the star in one of the young moving groups. The vertical velocity dispersion in the solar vicinity is only dependent on the scale height (Toth & Ostriker 1992). Old stars (2–10 Gyr) present higher scale heights than young stars (<1 Gyr), and hence high

* Based on observations made with the 2.2 m telescope of the German-Spanish Astronomical Centre, Calar Alto (Almería, Spain), operated jointly by the Max-Planck-Institute for Astronomy, Heidelberg, and the Spanish National Commission for Astronomy; the Nordic Optical Telescope (NOT), operated on the island of La Palma jointly by Denmark, Finland, Iceland, Norway and Sweden, in the Spanish Observatorio del Roque de Los Muchachos of the Instituto de Astrofísica de Canarias; the Isaac Newton Telescope (INT) operated on the island of La Palma by the Isaac Newton Group in the Spanish Observatorio del Roque de Los Muchachos of the Instituto de Astrofísica de Canarias; with the Italian Telescopio Nazionale Galileo (TNG) operated on the island of La Palma by the Centro Galileo Galilei of the INAF (Istituto Nazionale di Astrofisica) at the Spanish Observatorio del Roque de Los Muchachos of the Instituto de Astrofísica de Canarias; and with the Hobby-Eberly Telescope (HET) operated by McDonald Observatory on behalf of The University of Texas at Austin, the Pennsylvania State University, Stanford University, Ludwig-Maximilians-Universität München, and Georg-August-Universität Göttingen. This research has made use of the SIMBAD database and VizieR catalog access tool, operated at CDS, Strasbourg, France.

** Tables A.1–A.4 and reduced spectra are also available in electronic form at the CDS via anonymous ftp to cdsarc.u-strasbg.fr (130.79.128.5) or via <http://cdsweb.u-strasbg.fr/cgi-bin/qcat?J/A+A/514/A97>

values of W are more typical of old stars. However, the division between high and low velocity is subtle.

From the classical point of view of the Galactic velocity ellipsoid, early-type stars show lower dispersion in their Galactic velocities (U , V , and W) than late-type stars and are usually restricted to the spiral arms or star-forming regions. This result has already been interpreted in the past as a consequence of the increase of dispersion with increasing age (see [Mihalas & Binney 1981](#)). A recent study of the kinematics of M dwarfs in the solar vicinity by [Bochanski et al. \(2005\)](#) shows that the most chromospherically active (i.e. youngest) stars really show lower velocity dispersion than non-active (i.e. older) stars. Because of this and their ubiquity, late-type stars are excellent tracers of the Galactic potential ([Bochanski et al. 2007](#)). Distinguishing between young and old stars is then crucial to an understanding of the kinematics of the Galaxy and of stellar formation history in our neighborhood ([López-Santiago et al. 2007](#)).

An effort has been made in the past to quantify the proportion of young and old stars in samples of candidates of the young moving groups and associations using different age indicators. In particular, the level of magnetic activity is a powerful tool for this purpose (see [López-Santiago et al. 2009](#)). The activity level of late-type stars is inversely correlated with age due to the decrease of stellar rotation with increasing age (e.g. [Skumanich 1972](#); [Noyes et al. 1984](#); [Rutten & Schrijver 1987](#); [Randich et al. 1996](#); [Pizzolato et al. 2003](#)). The rotation-age-activity relationship persists into the fully convective regime (e.g. [Reiners & Basri 2007](#); [West et al. 2008](#)). M dwarfs indeed have finite active lifetimes ([West et al. 2009](#)). Therefore, the level of magnetic activity is a good indicator of age for late-F to M dwarfs.

For four years, between 1999 and 2002, our group carried out a spectroscopic survey of chromospherically active late-type stars in the solar neighborhood, selected from a list of possible members of classical young stellar kinematic groups ([Montes et al. 2001a](#)). The aim was to use different age indicators (chromospheric activity, lithium, rotational velocity) to constrain some properties of the moving groups and to study in detail the existence of age subgroups in large samples of stars selected, mainly, by their kinematics. Since then, the information derived from this project has been extensively used by us in different works. For instance, [Montes et al. \(2001b\)](#) carried out a multi-wavelength study of a sample of active stars, which allowed us to constrain the age of 14 young late-type stars. The results put constraints on the age of some young moving groups. Also, [López-Santiago et al. \(2003\)](#) studied the relation between variations observed in the photosphere and chromosphere of PW And using data from this spectroscopic survey.

More recently, part of the data from this survey was used to investigate nearby young moving groups ([López-Santiago et al. 2006](#)). A consequence of this study was the confirmation of the existence of two age subgroups in the previously discovered AB Dor moving group ([Zuckerman et al. 2004](#)). Through age indicators (mainly chromospheric activity and lithium abundance), we showed that the Local Association is indeed a mixture of subgroups of stars with different ages. In [López-Santiago et al. \(2009\)](#), we used the information on the chromospheric activity of the stars provided by the spectroscopic survey, together with X-ray data from the ROSAT All Sky Survey (RASS) to quantify the contamination by old main-sequence stars of the sample of possible members of the Local Association in [Montes et al. \(2001a\)](#).

At present, two projects are being progressed by our group based on the stars in this survey: studying the connection between various chromospheric activity indicators and the star

formation process in the chromosphere (see some preliminary results in [López-Santiago et al. 2005](#); [Crespo-Chacón et al. 2005](#)); and determining abundances of different elements in each star of the sample.

In this paper, we compile data derived by us for the stars observed in our survey. Our aim is to make the spectroscopic data accessible to the scientific community for future studies. In this new era of Virtual Observatory and extensive photometric databases and catalogs, the compilation of spectroscopic data is important for the purpose of constraining the properties of different astronomical objects, in particular, of stars (e.g. [Sciortino et al. 1995](#); [Takeda et al. 2007](#); [Micela et al. 2007](#); [López-Santiago et al. 2007](#); [Klutsch et al. 2008](#); [López-Santiago et al. 2009](#)). The utility of substantial spectroscopic compilations has been demonstrated in the past by various groups. For instance, the Geneva-Copenhagen group derived metallicities, ages and kinematics from spectroscopic observations of a very large sample of F to K-type (FGK) stars of the solar neighborhood ([Nordström et al. 2004](#)). These data were then used to investigate relations between metallicity, kinematics and age in the context of the evolution of the Galactic disk ([Nordström et al. 2004](#); [Holmberg et al. 2007, 2009](#)). Also, [Fuhrmann \(2004, 2008\)](#) determined spectroscopic parameters (temperature, gravity, metallicity, mass) of FGK stars in the solar vicinity with the aim of constructing an unbiased sample of stars in the Galactic thin and thick disk. Similarly, [Allende Prieto et al. \(2004\)](#) assembled a catalog of metallicities of late-type stars less than 25 pc from the sun.

Several spectroscopic surveys were performed mainly to study the evolution of magnetic activity with age in late-type stars, or simply to investigate chromospheric activity in general. Thus, the Palomar/MSU group compiled an extensive sample of nearby M stars and determined both kinematics ([Reid et al. 1995](#)) and chromospheric activity ([Hawley et al. 1996](#)). The data were also used to study the star formation history and luminosity function of the solar neighborhood ([Gizis et al. 2002](#); [Reid et al. 2002](#)). Another study on chromospheric emission is that of [Rauscher & Marcy \(2006\)](#), who measured Ca II H & K in a large sample of K7-M stars. Some groups are carrying out studies on how variations in line profiles produced by chromospheric activity affect the detection of planets. These studies are producing new catalogs of natural targets of planet searches with chromospheric emission measurements (e.g. [Martínez-Arnáiz et al. 2010](#), and references therein).

Other surveys have specifically focused on determining spectroscopic parameters of active stars. For instance, [Strassmeier et al. \(2000\)](#) presented measurements of equivalent widths of Ca II H & K, H α , and Li I in addition to the kinematics of a substantial sample of active and inactive FGK stars. Also, [Torres et al. \(2006\)](#) and [Guillout et al. \(2009\)](#) determined kinematics and age indicators in comprehensive samples of late-type stars to select members of young moving groups and associations. [White et al. \(2007\)](#) determined the same parameters for stars in the *Spitzer* Legacy Science Program “The Formation and Evolution of Planetary Systems”, aimed at studying the formation and evolution of protoplanetary disks. And [Shkolnik et al. \(2009\)](#) performed a spectroscopic survey of young M dwarfs within 25 pc. As [Valenti & Fischer \(2005\)](#) demonstrated in their spectroscopic analysis of effective temperature, surface gravity, metallicity, projected rotational velocity and abundance of 1040 nearby FGK stars, the use of automated tools provides uniform results and makes the analysis of large samples practical.

We determine here equivalent widths and fluxes of most of the chromospheric activity indicators from Ca II H & K to

the Ca II infrared triplet (including the Balmer series and the Na I doublet and Mg I triplet) in a sample of stars of the spectral types F to M. In this sense, our study implies an extension in terms of both spectral type range and wavelength coverage. We use the subtraction technique to subtract the photospheric contribution from the observed spectra, avoiding the use of calibrations to determine chromospheric emission. This approach represents an advance on previous studies. Together with the kinematics, rotation, and equivalent widths of Li I determined in this work, the sample constitutes an excellent laboratory for understanding the formation and evolution of the solar neighborhood during the past billion years.

The structure of the paper is as follows: in Sect. 2 we give details of the sample selection, the observations, and the data reduction methodology. In Sect. 3 we describe how we determined each parameter from the spectra. A brief summary of the results is given in Sect. 4. The Appendix contains tables with all the data and some figures with the spectra of stars in terms of selected chromospheric and photospheric features.

2. Sample selection, observations and data reduction

Our sample contains a total of 144 late-type stars. We selected 105 single stars from Montes et al. (2001a). Due to their membership in any of the moving groups studied in Montes et al. (2001a) (see Sect. 3.2 for a more detailed discussion on the stellar kinematic groups), we were quite certain that they are young and present chromospheric emission lines. Although late-type K and M stars remain active for a long period of their life (e.g. West et al. 2008), adding the condition of being member of a young moving group places a greater restriction on a star's age. Nevertheless, since the Montes et al. (2001a) sample also contains some old stars (López-Santiago et al. 2009), several stars of our present work could be older than ~ 1 Gyr. The remaining 39 stars of our sample were selected because they showed a high level of magnetic activity, rotational rate, and/or lithium abundance. A complete list of the stars observed by us is given in Table 1. The sample is restricted in declination since the observations were taken in telescopes sited in the Northern Hemisphere. The minimum declination reached is approximately -20° . Another restriction is the brightness of the star. Since *echelle* spectrographs have low efficiency, only stars with approximately $V \leq 12$ mag were selected. Our aim was to obtain spectra with high S/N even for the faintest stars (70–200 in the region of $H\alpha$). Spectral-type reference stars and radial velocity standards, used to determine the chromospheric excesses and heliocentric velocities of our stars, were also observed in each campaign. To obtain robust results, we ensured good spectral-type coverage in each observing run. A complete list of these stars is given in Table A.1.

The observations were carried out during twelve observing runs between 1999 and 2002. We used high resolution *echelle* spectrographs (resolving power, $\lambda/\Delta\lambda$, ranging from 30 000 to 60 000 at 6500 Å, $\Delta\lambda \sim 0.15$ Å), with the exception of one observing run, where we used a long-slit spectrograph with spectral resolution $\Delta\lambda = 1.13$ Å. Eighteen stars were observed with the latter configuration, nine of them were observed only during this observing run. For these nine stars, we determined only radial and rotational velocities and measured equivalent widths of Li I when possible. In general, errors in the measurements are only slightly larger for these stars than for those observed with higher resolution (see Table A.2). However, the low resolution

of the spectra in this observing run prevented us from measuring chromospheric emission in these nine stars to compare with our high resolution spectra (see Walkowicz & Hawley 2009, for a discussion on this issue). Details of each observing run are given in Table 2: date, telescope, spectrograph, CCD chip, spectral range covered, number of orders included in each *echelle* spectrum, range of reciprocal dispersion and spectral resolution (determined as the full width at half maximum, *FWHM*, of the arc comparison lines). Some of the stars were observed more than once (in the same campaign or even in different ones). The total number of spectra collected for this survey is 518 for targets and more than 50 for standards.

For data reduction, we used the standard procedures in the IRAF¹ package (bias subtraction, extraction of scattered light produced by optical system, division by a normalized flat-field and wavelength calibration). After reduction, each spectrum was normalized to its continuum, order by order, by fitting a polynomial function.

3. Results

3.1. Radial velocities

Heliocentric radial velocities were determined with the cross-correlation technique. In each observing run, the spectrum of each star was cross-correlated order by order against spectra of radial velocity standards of similar spectral type (stars marked with an asterisk in Table A.1) with the routine `fxcor` in IRAF. For each observed spectrum, radial velocities were derived for different spectral orders from the position of the peak of the cross-correlation function (CCF) by fitting a Gaussian to the function. Then, weighted means were calculated with the individual values obtained for each spectral order. To avoid systematic errors produced by the effect of cool spots in the CCF, we fitted the Gaussian to the entire CCF profile, instead of fitting only the peak.

Our results are listed in Table A.2. We give radial velocities for each observation of the star (V_r) and a mean velocity determined from the individual results for each observation (\overline{V}_r). Although our sample was selected from a list of single stars, some of them are actually single-line spectroscopic binaries. Known binaries in our sample are: HD 16525, HD 17190, HD 17382, HD 140913, HD 167605, HIP 89874² and HD 208472. During our observations, other stars presented variations in their radial velocities that were hardly attributable to spots. If caused by spots, they should produce noticeable asymmetries in the absorption line profiles, which was not observed in their spectra. For other stars, we determined radial velocities that were quite different from those given in the literature. Therefore, we classified all these stars as possible binaries: BD+28 1779, HD 85270, GJ 466, HD 112542, HD 112733, HD 238224, HD 160934, BD-05 5480, and GJ 842.2. The star HD 160934 was confirmed as a binary system by Hormuth et al. (2009) with preliminary orbital parameters determined by Gálvez et al. (2006).

Variations in the radial velocity measurements of up to several kilometers per second are induced in the CCF by asymmetries caused by spots on the stellar disk. This was even

¹ IRAF is distributed by the National Optical Observatory, which is operated by the Association of Universities for Research in Astronomy, Inc., under contract with the National Science Foundation.

² HIP 89874 (FK Ser) is a binary with a separation of 1.33 arcsec (Herbig & Bell 1988; Jensen et al. 1996). In our spectra, we were not able to separate the two components.

Table 1. Late-type stars studied in this work (HD number or other name).

166	1405	1326	1835	2410	QT And	4568	4614	4614 B
BD+17 232	12230	13382	16525	17190	17382	17925	17922	18632
18803	20678	21845	23232	24916	25457	25680	25998	25665
29697	30652	33564	36869	37394	233153	41593	TYC 1355-75-1	BD+20 1790
HIP 39721	GJ 9251B	HIP 39896	72905	73171	77191	77407	82558	82443
HIP 47176	HIP 49544	HIP 50156	GJ 388	HIP 51317	85270	98736	GJ 426B	102392
105631	238087	238090	106496	HIP 60661	110010	HIP 62686	HIP 63023	112542
112733	115043	HIP 65016	238224	117860	HIP 67092	125161B	129333	133826
134319	135363	140913	142764	143809	145675	146696	147379A	147379B
HIP 79796	149661	149931	152863	152751	155674A	155674B	156984	HIP 84794
HIP 85665	160934	162283	HIP 87579	HIP 87768	GJ 698B	165341	GJ 702B	167605
234601	SAO 9067	168442	HIP 89874	171488	171746	173739	173740	2RE J1846+191
GJ 734B	184525	187458	187565	191011	HIP 101262	197039	HIP 102401	198550
200560	200740	201651	HIP 104383	EUVE J2113+04.2	HIP 105885	HIP 106231	205435	206860
208472	HIP 108467	HIP 108752	TYC1680-01993-1	209458	HIP 109388	V383 Lac	GJ 856B	213845
BD+17 4799	HIP 112460	216899	217813	HIP 114066	220140	221503	HIP 117779	HIP 118212

Table 2. Observing run details.

Id.	Date	Telescope	Instrument	CCD chip	Spectral range (Å)	Orders	Dispersion (Å)	<i>FWHM</i> (Å)
1	1999 Jul. 24–29	2.2 m ^a	FOCES ¹	2048 × 2048 15 μm LORAL#11	3910–9075	84	0.03–0.07	0.09–0.15
2	1999 Nov. 26–27	NOT ^b	SOFIN ²	1152 × 770 EEV P88200	3525–10 425	44	0.06–0.17	0.14–0.32
3	2000 Jan. 18–22	INT ^c	MUSICOS ³	1024 × 1024 24 μm TEK5	4430–10 225	73	0.07–0.15	0.16–0.30
4	2000 Aug. 05–11	INT ^c	MUSICOS ³	1024 × 1024 24 μm TEK5	4430–10 225	73	0.07–0.15	0.16–0.30
5	2000 Nov. 10–13	NOT ^b	SOFIN ²	1152 × 770 EEV P88200	3525–10 425	44	0.06–0.17	0.14–0.32
6	2001 Apr. 02–05	INT ^c	IDS ⁴	2148 × 4200 13.5 μm EEV10a	3554–7137	1	0.48	1.22
7	2001 Sep. 21–24	2.2 m ^a	FOCES ¹	2048 × 2048 24 μm Site#1d	3510–10 700	112	0.04–0.13	0.08–0.35
8	2001 Oct. 10–11	TNG ^d	SARG ⁵	2(2048 × 4096) 13.5 μm EEV 4280	4960–10 110	62	0.02–0.04	0.08–0.17
9	2001 Dec. 19– 2002 Feb. 28	HET ^e	HRS ⁶	2(2048 × 4096) 15 μm Marconi	5040–8775	52	0.06–0.11	0.15–0.28
10	2002 Apr. 22–25	2.2 m ^a	FOCES ¹	2048 × 2048 24 μm Site#1d	3510–10 700	112	0.04–0.13	0.08–0.35
11	2002 Jul. 01–06	2.2 m ^a	FOCES ¹	2048 × 2048 24 μm Site#1d	3510–10 700	112	0.04–0.13	0.08–0.35
12	2002 Aug. 21–29	NOT ^b	SOFIN ²	2048 × 2048 2K3EB PISKUNOV1	3525–10 200	42	0.02–0.05	0.05–0.15

Notes. ^(a) 2.2 m telescope at German Spanish Astronomical Observatory (CAHA) (Almería, Spain); ^(b) 2.56 m Nordic Optical Telescope (NOT) at Observatorio del Roque de los Muchachos (La Palma, Spain); ^(c) 2.5 m Isaac Newton Telescope (INT) at Observatorio del Roque de los Muchachos (La Palma, Spain); ^(d) 3.5 m Telescopio Nazionale Galileo (TNG) at Observatorio del Roque de los Muchachos (La Palma, Spain); ^(e) 9.2 m Hobby-Eberly Telescope (HET) at McDonald Observatory (Texas, USA).

⁽¹⁾ FOCES: Fiber Optics Cassegrain Echelle Spectrograph; ⁽²⁾ SOFIN: Soviet Finnish High Resolution Echelle Spectrograph; ⁽³⁾ MUSICOS: spectrograph developed as part of Multi-Site COntinuous Spectroscopy project; ⁽⁴⁾ IDS: Intermediate Dispersion Spectrograph; ⁽⁵⁾ SARG: Spettrografo di Alta Risoluzione Galileo; ⁽⁶⁾ HRS: High Resolution Spectrograph.

then the case when a fit to the entire cross-correlation profile was performed (Dempsey et al. 1992; Strassmeier et al. 2000; López-Santiago et al. 2003). We observed variations of this order for several stars in our sample for which we took spectra during different nights of the same observing run: HD 1405, BD+17 232, BD+20 1790, HD 72905, HD 82558, AD Leo, HD 135363, HD 171488, V383 Lac and HD 220140.

In Table A.2 we also give the photometric periods available in the literature for some of the stars in the sample.

3.2. Space motion

Galactic space-velocity components (U , V , W) were determined as in Montes et al. (2001a), who used a modified version of the original procedure of Johnson & Soderblom (1987) to calculate Galactic velocities and associated uncertainties. As in Montes et al. (2001a), we did not correct (U , V , W) for solar motion to make comparisons with other works regarding moving groups easier. We used Hipparcos and Tycho-2 data (ESA 1997; Høg et al. 2000) and radial velocities determined by us.

For the ten stars with no available distance measurements in the literature, we determined a spectroscopic parallax using information on spectral type and luminosity class from our spectra. The Schmidt-Kaler (1982) color–magnitude relations were used to determine M_V for these stars. Note that for late-K and M stars, classic relations are not appropriate for determining some observed quantities. In particular, better spectroscopic parallax relations have been developed in the literature using molecular bands (e.g. Bochanski et al. 2005). Nevertheless, the spectral types of the stars in our sample for which we have determined a spectroscopic parallax are in the range F5–K3. Note also that small variations in the parallax (<10 mas) of stars produce only small variations in the Galactic velocities (<0.1 km s⁻¹).

The resultant U , V and W velocity components are listed in Table A.2. We used the mean radial velocity determined by us (\bar{V}_r in the table) for this computation. For the possible binary systems, we did not correct for binarity, because their orbits are as yet unknown. Thus, we used the observed radial velocities – or the mean value when more than one observation was performed – as a first approximation.

As we mentioned in Sect. 2, most of the stars in our sample (105) were selected from Montes et al. (2001a), who give a list of members and possible members of the young moving groups. For these, we obtained Galactic velocity components very similar to those given in Montes et al. (2001a). The remaining 39 stars of our sample had no previous measurement of UVW velocities. As a first estimate from their position in the UV - and WV -plane, 50 stars could be classified as members or possible members of the Local Association (in its various subgroups), 25 of the Hyades Supercluster, 20 of the Ursa Major Moving Group, 9 of the IC 2391 Supercluster, 5 of the Castor Moving Group, and the other 17 as young disk stars with no clear membership (see Table A.2). The same velocity dispersion as in Montes et al. (2001a) was used for determining the membership of the stars in any of the moving groups. We refer the reader to that paper for a detailed explanation. Surprisingly, 18 stars are well outside the classical boundaries of the young disk population in the UV -plane. Most of them are the lowest active stars in our sample, but two of them are very active stars: HIP 79796 and HD 216899 (see Figs. A.1–A.4).

3.3. Rotational velocities

To determine the rotational velocities in our sample, we used a methodology based on the cross-correlation technique, as we did for radial velocities (see Soderblom et al. 1989, for a detailed discussion). The width of the peak of the CCF depends on the physical processes contributing to the line profile. The mathematical concept is very similar to that of the convolution of a theoretical spectrum with a rotation profile (see Gray 2005, for details). But, instead of comparing the stellar spectrum with a rotationally broadened one, the cross-correlation is performed between the spectrum of the *program* star and a non-rotating one observed with the same instrument. Best results are obtained when both the comparison and the program stars have similar spectral types.

For each reference (non-rotating) star observed with our sample we first calibrated the relation between the CCF width and $v \sin i$ value by cross-correlating the star with itself after rotationally broadening its spectrum at different velocities (with values ranging from 1 to 60 km s^{-1}). The result is a relation between CCF width and rotational velocity (see Fig. 1). The relation depends on the spectral type of the star (as shown in the figure). Then we cross-correlated the program star with a standard with similar spectral type and used the relation for this standard to determine the rotational velocity of the program star. Since the relation also depends on the instrumental configuration, the cross-correlation was performed separately in each observing run. A detailed explanation of the method can be found in López-Santiago et al. (2003). For our study, the CCF peak width was determined by fitting a Gaussian function to it. This method ensures good results for $v \sin i \leq 50 \text{ km s}^{-1}$ (Soderblom et al. 1989). In our sample, there is only one star with $v \sin i > 50 \text{ km s}^{-1}$ (LO Peg). For this star, we determined its rotational velocity by comparison with artificially broadened spectra of different stars with similar spectral types.

In Table A.2, we give each value of $v \sin i$ obtained for the stars in the sample and a mean value determined from the individual results. Uncertainties were determined with the parameter R defined by Tonry & Davis (1979) as the ratio of CCF height to the rms antisymmetric component. This parameter is computed by `fxcor` and provides a measurement of the signal-to-noise ratio of the CCF. Tonry & Davis (1979) showed that errors in the CCF width are proportional to $(1 + R)^{-1}$,

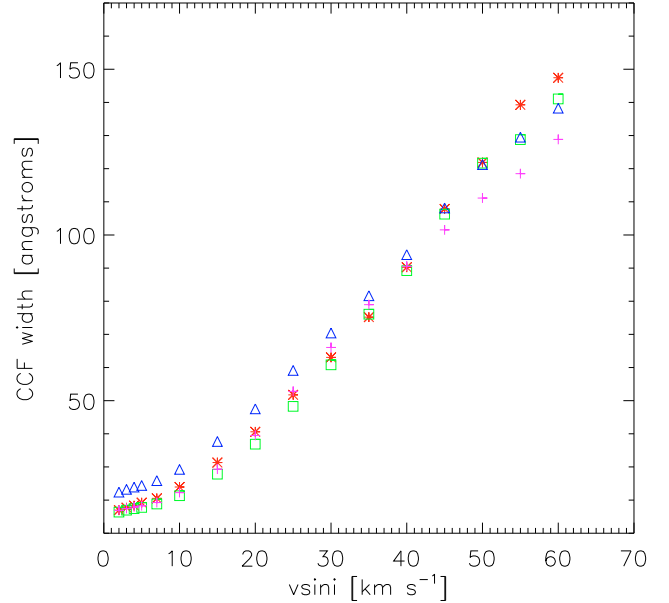


Fig. 1. CCF width – $v \sin i$ relation for standard stars of different spectral type in the same observing run: HD 182488 (G8V, asterisks), HD 185144 (K0 V, squares), HD 166620 (K2V, plusses), and HD 201091 (K5V, triangles).

while Hartmann et al. (1986) and Rhode et al. (2001) found that the quantity $\pm v \sin i (1 + R)^{-1}$ provides a good estimate for the 90% confidence level of the $v \sin i$ measurement. Thus we adopted $\pm v \sin i (1 + R)^{-1}$ as a reasonable estimate of the uncertainties in our determinations.

3.4. Spectral types and the lithium line

During each observing run, a number of spectral-type standards were observed, covering the range of spectral types in our sample (from F to M). To determine spectral types, we performed fits of our sample stars to spectral-type standards with a modified version of STARMOD (Barden 1985, see Sect. 3.5 for a detailed description of the procedure). The software first rotationally broadens the spectrum of the standard star until the best fit is obtained. Then it subtracts the obtained synthetic spectrum from the sample star. In theory, if both stars have the same spectral type, the resultant (subtracted) spectrum should be null. In practice, the subtracted spectrum shows some noise, due to small differences in metallicity and/or gravity and also when the S/N of one of the spectra is low. Nevertheless, small differences in metallicity and gravity are lower than those produced by the difference of one spectral subtype. The procedure of fitting is repeated with each of the standard stars until the best result is obtained. Errors are estimated in one spectral subtype.

Lines sensitive to spectral type were also used to determine spectral type. In particular, we used the lines Fe I $\lambda 6430 \text{ \AA}$, Fe II $\lambda 6432$ and 6457 \AA , Ca I $\lambda 6449$ and 6456 \AA , Co I $\lambda 6455 \text{ \AA}$, and V I $\lambda 6452 \text{ \AA}$, as described in Strassmeier & Fekel (1990). Other spectral lines used in this work for spectral classification are the Mg I triplet $\lambda 5167$, 5172 , and 5183 \AA , the Na I doublet $\lambda 5590$ and 5596 \AA , Ca I $\lambda 6573 \text{ \AA}$ and Fe I $\lambda 6575 \text{ \AA}$. In contrast to the subtraction technique, this method is suitable only for slow rotators, since the lines involved in each relation of Strassmeier & Fekel (1990) are blended in stars with high rotational velocities. Note that the relations are calibrated only for

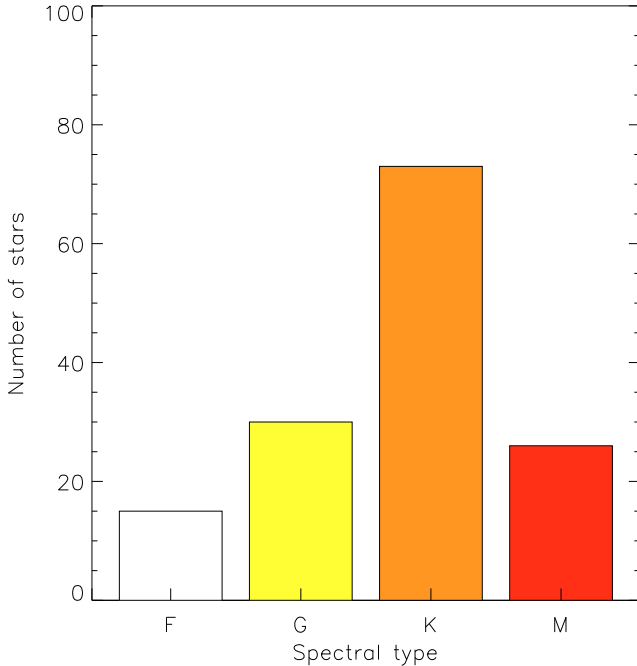


Fig. 2. Spectral type distribution of the stars in the sample.

FGK stars, but not for M ones. We used this method to test the results obtained with the subtraction technique for the stars in our sample showing small values of $v \sin i$. The most significant differences are two spectral subtypes for F stars and one subtype for G and K stars. These values are inside the uncertainties of the relations of [Strassmeier & Fekel \(1990\)](#). Our final results are given in [Table A.2](#) (see also [Fig. 2](#)).

We measured the equivalent width of the lithium line at 6707.8 \AA in the observed spectra. The lithium abundance is an appropriate age indicator for approximately $\log \text{age} \leq 8.8 \text{ Myr}$ (the age of the Hyades cluster) because this element is easily destroyed by thermonuclear reactions in the stellar interior. Thus detection of the lithium line is generally a sign of stellar youth in single stars (high rotation velocities could preserve the lithium from depletion over longer time scales in binaries). The lithium-age relation is mass-dependent. The usual way to determine the age range is by comparison with stars of similar spectral type in clusters of a well-known age (e.g. [Soderblom & Mayor 1993](#); [Neuhäuser et al. 1997](#); [Montes et al. 2001b](#)). In our spectra, the $\text{Li I } \lambda 6707.8 \text{ \AA}$ line is blended with the $\text{Fe I } \lambda 6707.4 \text{ \AA}$ line. To correct the measured equivalent width ($EW[\text{Li I} + \text{Fe I}]$) for the Fe I line, we used the empirical relationship of [Soderblom et al. \(1993\)](#). The results are given in [Table A.2](#). An error-weighted mean value of the individual $EW[\text{Li I}]$ measured on different nights and over different observing runs was also determined (see [Table A.2](#)). Many stars in the sample still show the Li I absorption line in their spectra (see [Table A.2](#) and [Fig. A.3](#)). Some of them are very young ($\log \text{age} \leq 7.5 \text{ Myr}$). They belong to the young stellar associations ([Zuckerman et al. 2004](#); [Torres et al. 2008](#)). In particular, [López-Santiago et al. \(2006\)](#) established different age subgroups in the AB Dor moving group using results from this study.

3.5. Chromospheric activity

A special feature of *echelle* spectrographs is that they cover a large fraction of the optical spectrum. It allows simultaneous

observations of all the activity indicators in this spectral range to be obtained. We measured equivalent widths of the chromospheric optical lines Ca II H & K, H ϵ , H δ , H γ , H β , H α , and the Ca II infrared triplet, for each observation of each star in our sample, when the spectrograph configuration permitted it. In very active stars (active M dwarfs and flare stars), we also measured equivalent widths of the lines He I $\lambda 5876 \text{ \AA}$ and the Na I doublet ($\lambda 5890, 5896 \text{ \AA}$).

To remove the photospheric contribution, we used the spectral subtraction technique (see details in [Montes et al. 2000](#)). The advantage of this method is that no assumption about the continuum value for the equivalent width measurement is needed. Reference (non-active) stars with similar spectral types to our targets were taken as templates (see [Table A.1](#)). The subtraction was performed with JSTARMOD, a modified version of the Fortran code STARMOD developed at the Pennsylvania State University ([Huenemoerder & Barden 1984](#); [Barden 1985](#)). Our modifications permit the program to use *echelle* spectra in the file format given by the majority of observatories. JSTARMOD first selects the region of the spectrum indicated by the user. Then it rotationally broadens and shifts the template spectrum to fit the target one. Finally it subtracts the synthetic spectrum from the observed one. If both stars – active and non-active – are identical in terms of photosphere, the resultant subtracted spectrum is the chromospheric emission of the active star, i.e. a flat spectrum with emission features at the positions of the chromospheric lines. In practice, the subtracted spectrum shows some noise away from the chromospheric lines, due to small differences in metallicity and/or gravity.

A source of uncertainties is the possible basal emission of the non-active stars used as templates. Its consequence is a reduction in the measured equivalent widths of the Ca II H & K chromospheric emissions of the target. However, for the subtraction we used reference stars situated close to the lower boundary of the surface flux in Ca II H & K of [Rutten \(1984\)](#). We estimate the largest uncertainty in logarithm fluxes as 0.1 dex, due to basal chromospheric emission from standard non-active stars.

The equivalent widths were determined by fitting a Gaussian function to the emission line profiles. For the Ca II H and H ϵ lines, which are blended in our spectra, we used a double Gaussian fit. To obtain an estimation of the errors, we followed the methodology explained in [López-Santiago et al. \(2003\)](#). Our results are given in [Table A.3](#). Each measurement of the equivalent width and its uncertainty is listed in the table, together with the observing run and the Modified Julian Date (MJD) of the observation. Equivalent widths were later converted to absolute chromospheric fluxes at the stellar surface with the calibrations of [Hall \(1996\)](#) (see results in [Table A.4](#)).

In [Fig. 3](#) we show the distribution of fluxes in different chromospheric lines (to allow statistical comparisons with other works). The sample has a peak towards high chromospheric fluxes in chromospheric calcium. Two peaks are observed in H α . The peak at high fluxes in each line is a consequence of the selection method. The double peak in H α is presumably caused by the presence of two populations of H α emitters: saturated and non-saturated. To verify this hypothesis, we constructed plots of the ratio $F_{\text{line}}/F_{\text{bol}}$ versus temperature for each chromospheric line. In [Fig. 4](#), we show the result for H α and the Ca II $\lambda 8542 \text{ \AA}$ (IRT2) line. Two well-defined branches are observed for H α . A similar behavior was observed for coronal sources (e.g. [López-Santiago et al. 2009](#)) and was attributed to X-ray emission saturation. Similarly, the stars in our sample show saturation in H α at a mean value $\log F_{\text{H}\alpha}/F_{\text{bol}} \sim -3.8$,

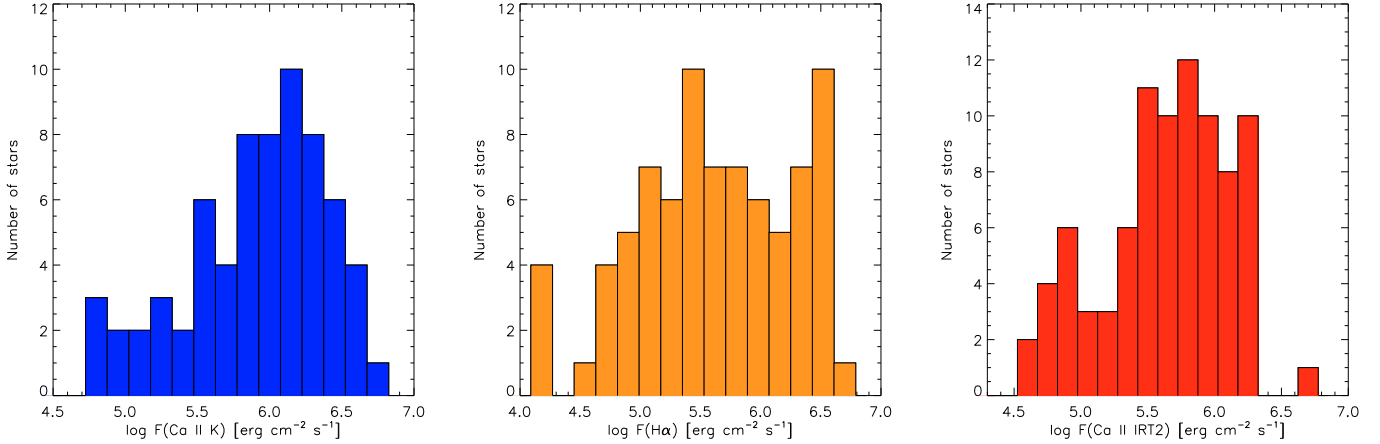


Fig. 3. Histograms for results on some chromospheric activity indicators (absolute flux after subtraction of the photosphere).

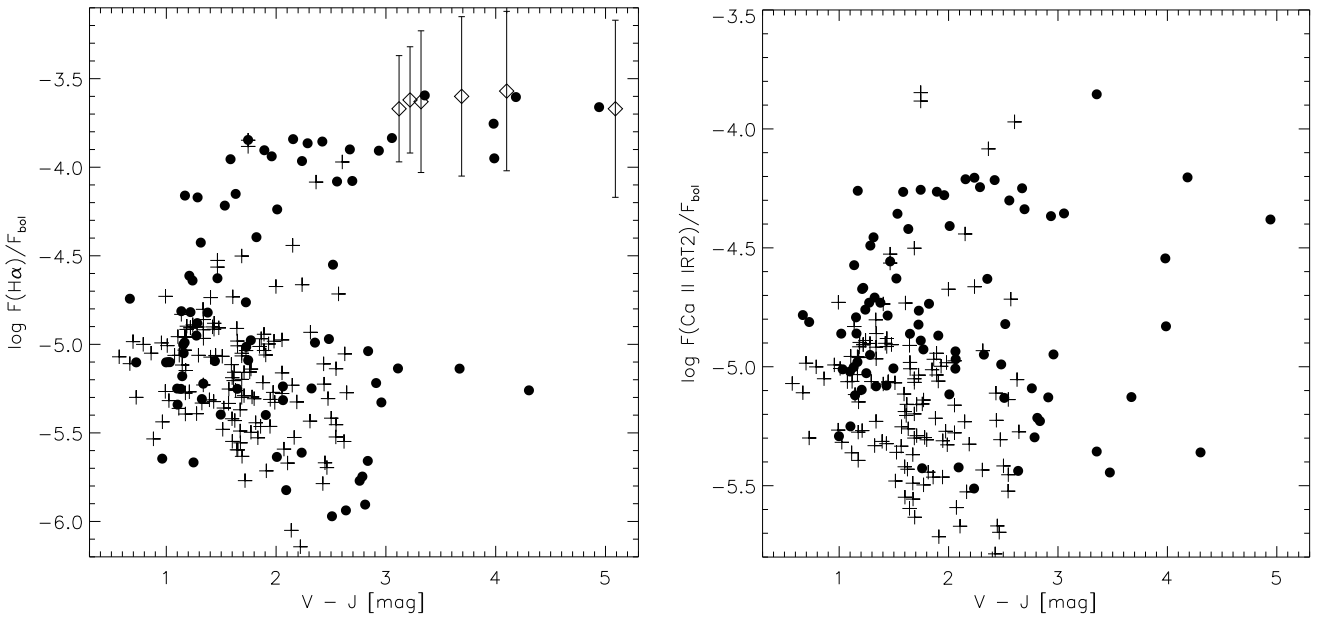


Fig. 4. *Left:* $\log F_S(\text{H}\alpha)/F_{\text{bol}}$ versus $V - J$ for the stars in our sample (dots). Plusses are the stars in Martínez-Arnáiz et al. (2010). Diamonds are the data of West et al. (2004). *Right:* $\log F_S(\text{Ca II } \lambda 8542 \text{ \AA})/F_{\text{bol}}$ versus $V - J$ of the stars in our sample. Symbols are the same as in the left figure.

as was found for early to mid-M stars (e.g. Walkowicz et al. 2004; West et al. 2008). The effect of saturation is less marked in other indicators, like the Ca II lines (see Fig. 4, right).

In addition to the absolute fluxes in the different chromospheric lines we also determined the R'_{HK} index (see Table A.4), which is defined as the ratio of the emission from the chromosphere in the Ca II H & K lines to the total bolometric emission of the star, i.e.

$$R'_{\text{HK}} = \frac{F'_H + F'_K}{\sigma T^4}, \quad (1)$$

where F'_H and F'_K are the chromospheric fluxes in the Ca II H and K lines, respectively. Effective temperatures were determined through empirical calibrations with the color index $B - V$ (e.g. Gray 2005). These calibrations are valid for $B - V \leq 1.5$. Only seven stars of our sample (three of them being giants) have values of $B - V$ above 1.5. For these, we extrapolated the color-temperature relation. For $B - V > 1.5$, the spread in temperatures is wide (see Fig. 14.6 in Gray 2005). Differences between the value given by the relation and that obtained with other

methods (e.g. Flower 1996) of up to 100–200 K are observed for M dwarfs.

Figures A.1–A.3 show the spectra of the stars in the sample in spectral regions containing the Ca II K line, H α , and part of the Ca II infrared triplet.

3.6. Summary

Radial and rotational velocities were derived from each observation of a star in our sample with the cross-correlation technique. We derived mean radial and rotational velocities for each star. In some cases (see Sect. 3.1) we observed significant variations in the radial velocity of the star, which we attributed to binarity. Mean values of radial velocities were used to derive space motions. We also determined spectral types from the spectra of stars. Table A.2 summarizes these results.

With regard to spectral lines, we determined equivalent widths of all optical chromospheric activity indicators of each star as well as the Li I $\lambda 6708 \text{ \AA}$ line (see Table A.2 for results of the Li I line). To reveal chromospheric emission lines in the

spectra, we used the spectral subtraction technique. Non-active stars with spectral types similar to those of our targets were taken as templates for the subtraction. Their spectra were conveniently broadened and shifted to fit our targets (see Sect. 3.4). The equivalent widths of the emission lines were converted into flux using equivalent width-flux relations. Tables A.3 and A.4 summarize the results of the spectroscopic survey.

For completeness, we performed a simple statistical study of our results on chromospheric activity indicators. In our sample, a large spread in fluxes is observed for the different activity indicators. The spread is especially noticeable for the $H\alpha$ line (Fig. 3, middle). To investigate this finding, we analyzed the $F_{H\alpha}/F_{\text{bol}}$ and $F_{\text{CaII}}/F_{\text{bol}}$ ratios as a function of the color of the stars. The results indicate the presence of two populations of chromospherically active stars in our sample. In the $\log F_{H\alpha}/F_{\text{bol}} - (V - J)$ diagram (Fig. 4, left), two branches are clearly observed for $V - J \geq 1.4$ mag (corresponding to an early-K dwarf). This dichotomy is statistically significant. Out of the 79 stars in our sample with chromospheric $H\alpha$ emission, 53 have $V - J > 1.4$ with 23 stars in the upper branch and the remaining 30 in the lower one. The two groups have mean values $\log F_{H\alpha} = -3.9$ with variance 0.04 and $\log F_{H\alpha} = -5.3$ with variance 0.13, respectively. A simple two-sample t-test (e.g. [Snedecor & Cochran 1989](#)) assures that the two means are different (i.e. the two branches are statistically different), with a significance of 0.01 (corresponding to a probability of 99%). The presence of the two branches is less clear when using other chromospheric activity indicators (see Fig. 4, right).

In a recent work, [López-Santiago et al. \(2009\)](#) demonstrated that the sample of possible members of the young stellar kinematic groups of [Montes et al. \(2001a\)](#) is partially contaminated by active field stars that do not belong to the moving groups. In that work, the stars in the X-ray saturation regime also showed high $H\alpha$ fluxes. In their Fig. 4, [López-Santiago et al. \(2009\)](#) observed two branches: one for the high $H\alpha$ emitters and the other for the remaining active stars. Those stars populating the upper branch were indeed young (~ 10 – 120 Myr). In contrast, field stars populated the lower branch. The study of [López-Santiago et al. \(2009\)](#) was performed using part of the data presented by us in this work. Therefore their results on the nature of the two populations of chromospheric active stars are applicable here. In fact, the stars in the top branch in Fig. 4 (left) are known to be young stars (see [López-Santiago et al. 2006](#)) and very active M dwarfs. A similar conclusion was already reached by [Vaughan & Preston \(1980\)](#) for G and K stars. In their study, the authors observed two branches in the $\log S - (B - V)$ diagram with a gap between them. The authors called the active one the “young branch” and the less active one the “old branch”. Recent results show that this dichotomy between very active stars and less active ones is also present in M dwarfs. In Fig. 4 (left), we overplotted the data obtained by [West et al. \(2004\)](#) for the active M stars in the SLOAN Digital Sky Survey (the dispersion observed by the authors for each sub-spectral type is represented by vertical bars). Although our method for measuring the line flux is slightly different from that of [West et al. \(2004\)](#), the figure clearly shows that M active dwarfs are located over the young active branch. A similar trend can be observed for the early M dwarfs of [Reiners \(2007\)](#). In general, these results suggest that $H\alpha$ saturates equally in K to M stars.

Acknowledgements. Part of this work was co-supported by the Spanish MICINN, Ministerio de Ciencia e Innovación project numbers: AYA2008-00695 and AYA2008-06423-C03-03. J. López-Santiago is a postdoctoral fellow of the ASTROCAM (Red de Astrofísica en la CAM) with project number S-0505/ESP/000237 of the IV PRICIT Plan Regional de Investigación

Científica e Innovación Tecnológica de la Comunidad de Madrid. The authors would like to thank the referee for useful comments and suggestions that allowed us to improve our work.

References

- Allende Prieto, C., Barklem, P. S., Lambert, D. L., & Cunha, K. 2004, A&A, 420, 183
- Antoja, T., Figueras, F., Fernández, D., & Torra, J. 2008, A&A, 490, 135
- Antoja, T., Valenzuela, O., Pichardo, B., et al. 2009, ApJ, 700, L78
- Asiain, R., Figueras, F., Torra, J., & Chen, B. 1999, A&A, 341, 427
- Barden, S. C. 1985, ApJ, 295, 162
- Barnes, T. G., III, Moffett, T. J., & Slovak, M. H. 1986, PASP, 98, 223
- Beavers, W. I., Eitter, J. J., Ketelsen, D. A., & Oesper, D. A. 1979, PASP, 91, 698
- Benz, W., & Mayor, M. 1984, A&A, 138, 183
- Bochanski, J. J., Hawley, S. L., Reid, I. N., et al. 2005, AJ, 130, 1871
- Bochanski, J. J., Munn, J. A., Hawley, S. L., et al. 2007, AJ, 134, 2418
- Böhm-Vitense, E. 2007, ApJ, 657, 486
- De Medeiros, J. R., & Mayor, M. 1999, A&AS, 139, 433
- Crespo-Chacón, I., Montes, D., Fernández-Figueroa, M. J., & López-Santiago, J. 2005, in Proceedings of the 13th Cambridge Workshop on Cool Stars, Stellar Systems and the Sun, 5–9 July, 2004, Hamburg, Germany, ed. F. Favata, G. A. J. Hussain, & B. Battrick, European Space Agency, ESA SP-560, 491
- De Medeiros, J. R., Do Nascimento, J. D., Jr., Sankarankutty, S., Costa, J. M., & Maia, M. R. G. 2000, A&A, 363, 239
- Dempsey, R. C., Bopp, B. W., Strassmeier, K. G., et al. 1992, ApJ, 392, 187
- Dufflot, M., Figon, P., & Meyssonnier, N. 1995, A&AS, 114, 269
- Dyer, E. R., Jr. 1954, AJ, 59, 218
- ESA 1997, The Hipparcos and Tycho Catalogues, ESA SP-1200
- Famaey, B., Jorissen, A., Luri, X., et al. 2005, A&A, 430, 165
- Famaey, B., Pont, F., Luri, X., et al. 2007, A&A, 461, 957
- Fekel, F. C. 1997, PASP, 109, 514
- Flower, P. J. 1996, ApJ, 469, 355
- Fuhrmann, K. 2004, Astron. Nachr., 325, 3
- Fuhrmann, K. 2008, MNRAS, 384, 173
- Gálvez, M. C., Montes, D., Fernández-Figueroa, M. J., & López-Santiago, J. 2006, Ap&SS, 304, 59
- Gray, C. D. F. 2005, Stellar Photospheres (Cambridge: Cambridge University Press)
- Guillout, P., Klutsch, A., Frasca, A., et al. 2009, A&A, 504, 829
- Gizis, J. E., Reid, I. N., & Hawley, S. L. 2002, AJ, 123, 3356
- Hall, J. C. 1996, PASP, 108, 313
- Hartmann, L., Hewett, R., Stahler, S., & Mathieu, R. D. 1986, ApJ, 309, 275
- Hawley, S. L., Gizis, J. E., & Reid, I. N. 1996, AJ, 112, 2799
- Herbig, G. H., & Bell, K. R. 1988, in Catalog of emission line stars of the orion population, Lick Observatory Bulletin, Santa Cruz, Lick Observatory
- Hög, E., Fabricius, C., Makarov, V. V., et al. 2000, A&A, 355, L27
- Holmberg, J., Nordström, B., & Andersen, J. 2007, A&A, 475, 519
- Holmberg, J., Nordström, B., & Andersen, J. 2009, A&A, 501, 941
- Hormuth, F., Brandner, W., Hippler, S., et al. 2007, A&A, 463, 707
- Huenemoerder, D. P., & Barden, S. C. 1984, BAAS, 16, 510
- Jensen, E. L. N., Mathieu, R. D., & Fuller, G. A. 1996, ApJ, 458, 312
- Johnson, D. H., & Soderblom, D. R. 1987, AJ, 93, 864
- Klutsch, A., Frasca, A., Guillout, P., et al. 2008, A&A, 490, 737
- López-Santiago, J., Montes, D., Fernández-Figueroa, M. J., & Ramsey, L. W. 2003, A&A, 411, 489
- López-Santiago, J., Montes, D., Fernández-Figueroa, M. J., et al. 2005, in Proceedings of the 13th Cambridge Workshop on Cool Stars, Stellar Systems and the Sun, 5–9 July, 2004, Hamburg, Germany, ed. F. Favata, G. A. J. Hussain, & B. Battrick, ESA SP-560, European Space Agency, 775
- López-Santiago, J., Montes, D., Crespo-Chacón, I., & Fernández-Figueroa, M. J. 2006, ApJ, 643, 1160
- López-Santiago, J., Micela, G., Sciortino, S., et al. 2007, A&A, 463, 165
- López-Santiago, J., Micela, G., & Montes, D. 2009, 499, 129
- Marcy, G. W., & Chen, G. H. 1992, ApJ, 390, 550
- Martínez-Arnáiz, R., Maldonado, J., Montes, D., Eiroa, C., & Montesinos, B. 2010, A&A, in press [arXiv:1002.4391]
- Micela, G., Affer, L., Favata, F., et al. 2007, A&A, 461, 977
- Mihalas, D., & Binney, J. 1981 (San Francisco: W. H. Freeman and Co.), 422
- Montes, D., Fernández-Figueroa, M. J., De Castro, E., et al. 2000, A&AS, 146, 103
- Montes, D., López-Santiago, J., Gálvez, M. C., et al. 2001a, MNRAS, 328, 45
- Montes, D., López-Santiago, J., Fernández-Figueroa, M. J., & Gálvez, M. C. 2001b, A&A, 379, 976
- Neuhäuser, R., Torres, G., Sterzik, M. F., & Randich, S. 1997, A&A, 325, 647
- Nidever, D. L., Marcy, G. W., Butler, R. P., et al. 2002, ApJS, 141, 503
- Nordström, B., Mayor, M., Andersen, J., et al. 2004, A&A, 418, 989

Noyes, R. W., Hartmann, L. W., Baliunas, S. L., et al. 1984, *ApJ*, 279, 763
 Pizzolato, N., Maggio, A., Micela, G., et al. 2003, *A&A*, 397, 147
 Randich, S., Schmitt, J. H. M. M., Prosser, C. F., & Stauffer, J. R. 1996, *A&A*, 305, 785
 Rauscher, E., & Marcy, G. W. 2006, *PASP*, 118, 617
 Reid, I. N., Hawley, S. L., & Gizis, J. E. 1995, *AJ*, 110, 1838
 Reid, I. N., Gizis, J. E., & Hawley, S. L. 2002, *AJ*, 124, 2721
 Reiners, A. 2007, in Annual Meeting of the German Astronomical Society [arXiv:0712.2357]
 Reiners, A., & Basri, G. 2007, *ApJ*, 656, 1121
 Rhode, K. L., Herbst, W., & Mathieu, R. D. 2001, *AJ*, 122, 3258
 Rutten, R. G. M. 1984, *A&A*, 130, 353
 Rutten, R. G. M., & Schrijver, C. J. 1987, *A&A*, 177, 155
 Schmidt-Kaler, T. 1982, in Landolt-Bornstein, ed. K. Schaifers, & H. H. Voigt (Heidelberg: Springer), 2
 Sciortino, S., Favata, F., & Micela, G. 1995, *A&A*, 296, 370
 Shkolnik, E., Liu, M. C., & Reid, I. N. 2009, *ApJ*, 699, 649
 Skuljan, J., Hearnshaw, J. B., & Cottrell, P. L. 1999, *MNRAS*, 308, 731
 Snedecor, G. W., & Cochran, W. G. 1989, *Statistical Methods*, eighth edn. (Ames, Iowa: Iowa State University Press)
 Soderblom, D. R. 1982, *ApJ*, 263, 239
 Soderblom, D. R., & Mayor, M. 1993, *ApJ*, 402, L5
 Soderblom, D. R., Pendleton, J., & Pallavicini, R. 1989, *AJ*, 97, 539
 Soderblom, D. R., Jones, B. F., Balachandran, S., et al. 1993, *AJ*, 106, 1059
 Skumanich, A. 1972, *ApJ*, 171, 565
 Strassmeier, K. G., & Fekel, F. C. 1990, *A&A*, 230, 389
 Strassmeier, K. G., Hall, D. S., Fekel, F. C., & Scheck, M. 1993, *A&AS*, 100, 173
 Strassmeier, K. G., Washuettl, A., Granzer, Th., et al. 2000, *A&AS*, 142, 275
 Takeda, G., Ford, E. B., Sills, A., et al. 2007, *ApJS*, 168, 297
 Tokovinin, A. A. 1992, *A&A*, 256, 121
 Tonry, J., & Davis, M. 1979, *AJ*, 84, 1511
 Torres, C. A. O., Quast, G. R., da Silva, L., et al. 2006, *A&A*, 460, 695
 Torres, C. A. O., Quast, G. R., Melo, C. H. F., & Sterzik, M. F. 2008, *Handbook of Star Forming Regions, Volume II: The Southern Sky*, ASP Monograph Publications, ed. B. Reipurth, 5, 757
 Toth, G., & Ostriker, J. P. 1992, *ApJ*, 389, 5
 Udry, S., Mayor, M., Maurice, E., et al. 1999, in *Precise Stellar Radial Velocities*, ed. J. B. Hearnshaw, & C. D. Scarfe, IAU Colloq., 170, ASP Conf. Ser., 185, 383
 Valenti, J. A., & Fischer, D. A. 2005, *ApJS*, 159, 141
 Vaughan, A. H., & Preston, G. W. 1980, *PASP*, 92, 385
 Walkowicz, L. M., Hawley, S. L., & West, A. A. 2004, *PASP*, 116, 1105
 Walkowicz, L. M., & Hawley, S. L. 2009, *AJ*, 137, 3297
 West, A. A., Hawley, S. L., Walkowicz, L. M., et al. 2004, *AJ*, 128, 426
 West, A. A., Hawley, S. L., Bochanski, J. J., et al. 2008, *AJ*, 135, 785
 West, A. A., Hawley, S. L., Bochanski, J. J., et al. 2009, *IAU Symp.*, 258, 327
 White, R. J., Gabor, J. M., & Hillenbrand, L. A. 2007, *AJ*, 133, 2524
 Zuckerman, B., Song, I., & Bessell, M. S. 2004, *ApJ*, 613, L65

Appendix A: Description of the on-line material

- Table A.1: spectral-type reference stars and radial velocity standards used for the subtraction of the photospheric spectrum and for determining radial and rotational velocities. Column 1 is the name/identification of the star; Col. 2 is the

spectral type; Col. 3 is the radial velocity (and standard deviation); Col. 4 is the bibliographic reference for the radial velocity; Col. 5 is the rotational velocity (and standard deviation); Col. 6 is the bibliographic reference of the rotational velocity; Col. 7 is the activity index S (and standard deviation); and Col. 8 is the observing run in which the star was observed by us.

- Table A.2: spectroscopic parameters of the stars in the sample. Each line corresponds to a measurement/observation of the star. Column 1 is the HD number or other name of the star; Col. 2 is the observing run in which the observation was performed; Col. 3 is the Modified Julian Date of the observation; Col. 4 is the spectral type of the star determined by us; Col. 5 is the $B - V$ color from Tycho-2; Col. 6 is the radial velocity determined by us in that observation; Col. 7 is a mean radial velocity of every observation performed for the star; Cols. 8–10 are the Galactic velocities; Col. 11 is the rotational velocity determined in that observation; Col. 12 is a mean value of the rotational velocity of the star determined in each observation; Col. 13 is the photometric period found in the literature; Col. 14 is the equivalent width of the lithium line in 6707.8 \AA determined in that observation; Col. 15 is a mean value of the equivalent width of the lithium line of the star; and Col. 16 is the preliminary assignation to a moving group made by us in base to the Galactic velocity given in Cols. 8–10.
- Table A.3: equivalent widths of the different chromospheric lines determined in each observation from the subtracted spectrum. Column 1 is the identification of the star in our sample (the same as in Table A.2); Col. 2 is the observing run of the observation; Col. 3 is the Modified Julian Date of the observation; Cols. 4 to 16 are the equivalent widths in the chromospheric lines (in order): Ca II K & H, H ϵ , H δ , H γ , H β , He I D $_3$, Na I D $_2$ & D $_1$, H α , and Ca II infrared triplet ($\lambda\lambda 8498, 8542, 8662 \text{ \AA}$), with errors.
- Table A.4: surface fluxes of the different chromospheric lines determined in each observation from the equivalent widths in Table A.3. Column 1 is the identification of the star in our sample (the same as in Table A.2); Col. 2 is the observing run of the observation; Col. 3 is the Modified Julian Date of the observation; Cols. 4 to 16 are the surface fluxes in the chromospheric lines (in order): Ca II K & H, H ϵ , H δ , H γ , H β , He I D $_3$, Na I D $_2$ & D $_1$, H α , and Ca II infrared triplet ($\lambda\lambda 8498, 8542, 8662 \text{ \AA}$), with errors; Col. 17 is the R'_{HK} index.
- Figures A.1 to A.4: figures with the normalized spectrum of the stars in our sample in the spectral regions of the Ca II K, H α , Li I, and Ca II $\lambda\lambda 8498$ and 8542 \AA lines, respectively.

Table A.1. Spectral-type reference stars and radial velocity standards (marked with *).

HD/GJ	SpT	$V_r \pm \sigma_{V_r}$ (km s ⁻¹)	Ref _v	$v \sin i$ (km s ⁻¹)	Ref _r	$S \pm \sigma_S$	Observing run
212754	F7 V	-17.8 ± 1.2	a	7.9 ± 0.7	j	0.142 ± 0.001	4, 5
43587 *	F9 V	4.6 ± 0.1	b	...		0.158 ± 0.001	5, 6
84737 *	G0.5 V	6.0 ± 1.1	b	2.8 ± 0.8	j	0.144 ± 0.000	10
10307	G2 V	...		2.1 ± 0.5	k	0.152 ± 0.003	7
193664	G3 V	-4.7 ± 1.2	a	...		0.161 ± 0.004	7
25680	G5 V	24.0 ± 0.1	c	7.0 ± 0.7	j	0.281 ± 0.000	5, 7
31966	G5 V	-18.1 ± 0.1	c	5
71148 *	G5 V	-31.0 ± 0.7	b	...		1.570 ± 0.000	10
159222 *	G5 V	-50.5 ± 1.2	b	...		0.164 ± 0.002	1, 4, 11
182488 *	G8 V	-21.5	d	0.6 ± 0.5	k	0.155 ± 0.008	1, 4, 11
48432	K0 III	17.9 ± 0.2	e	<1.0	e	0.120 ± 0.000	5, 6
62509 *	K0 III	3.2 ± 0.3	b	1.7 ± 0.5	k	0.140 ± 0.019	3
100696 *	K0 III	0.2 ± 0.5	b	1.2 ± 1.0	l	...	10
197989	K0 III	-10.6 ± 0.5	a	2.0 ± 0.5	k	0.104 ± 0.001	1, 2, 4, 7, 8, 11
3651 *	K0 V	-32.8 ± 0.8	b	2.2 ± 0.5	k	0.191 ± 0.001	2, 3, 4, 5, 7
97004	K0 V	5.4 ± 0.1	c	10
112758	K0 V	-4.1 ± 1.2	a	...		0.206 ± 0.000	10
136442 *	K0 V	-45.6 ± 0.8	b	10
185144	K0 V	26.7 ± 0.1	c	0.6 ± 0.5	k	0.195 ± 0.003	11
201651	K0 V	-13.7 ± 1.2	a	4, 7, 8
92588 *	K1 IV	43.5 ± 0.3	f	<1.0	e	...	9, 10
10476 *	K1 V	-33.9 ± 0.9	b	0.6 ± 0.5	k	0.192 ± 0.001	1, 5
12929 *	K2 III	-14.6 ± 0.2	g	1.8 ± 0.5	k	0.118 ± 0.002	5
124897 *	K2 III	-5.3 ± 0.3	g	3.3 ± 0.5	k	0.144 ± 0.012	6, 10
161096 *	K2 III	-12.5 ± 0.3	g	2.5 ± 0.5	k	0.103 ± 0.002	1, 4, 11
201196	K2 IV	-34.8 ± 0.2	e	<1.0	e	...	1, 5
4628 *	K2 V	-10.1 ± 0.4	f	0.0 ± 0.5	h	0.223 ± 0.001	2, 5, 8, 12
136713	K2 V	-6.0 ± 0.1	c	3.8 ± 5.7	m	...	6
166620	K2 V	6.9 ± 0.1	h	0.0 ± 0.4	h	0.193 ± 0.001	1, 2, 4, 6, 7, 9, 10, 11
16160	K3 V	25.8 ± 0.1	c	1.0 ± 1.0	h	0.221 ± 0.002	8
219134	K3/4 V	-18.6 ± 0.1	c	2.1 ± 0.5	k	0.229 ± 0.003	1, 2, 4, 5, 11
29139 *	K5 III	54.2 ± 0.2	g	2.0 ± 1.0	e	...	4, 6, 7
154363	K5 V	34.1 ± 0.1	c	3.7 ± 5.9		0.197 ± 0.001	1, 6, 10
201091	K5 V	7.0 ± 0.1	h	0.0 ± 0.8	h	0.613 ± 0.006	1, 4, 5, 6, 7, 8, 10, 11
GJ 910	K5 V	2.0	i	0.0 ± 0.0	m	...	7
151877	K7 V	2.0 ± 0.1	c	0.0 ± 0.0	m	...	1
201092	K7 V	7.2 ± 0.1	h	1.7 ± 0.6	h	0.922 ± 0.011	1, 4, 5, 6, 7, 8, 10, 11
GJ 466	M0 V	-5.0 ± 5.0	a	10
147379	M0 V	-18.8 ± 0.1	c	4.2 ± 6.2	m	1.761 ± 0.160	11
GJ 720A	M0 V	-25.0 ± 2.5	a	6.3 ± 1.7	m	...	7
GJ 16	M0/1 V	8
GJ 806	M1.5 V	-24.7 ± 0.1	c	1.9 ± 0.7	n	...	11
18884 *	M2 III	-26.1 ± 0.3	g	...		0.331 ± 0.004	8
115521 *	M2 III	-28.6 ± 2.3	g	6, 10
95735	M2 V	-84.7 ± 0.1	c	0.0 ± 0.0	n	0.392 ± 0.009	6, 10
GJ 687B [†]	M3.5 V	-28.8 ± 0.1	c	6, 10

Notes. ^(†) The radial velocity given for GJ 687B is that of GJ 687A.

References. a Dufflot et al. (1995), WEB (Wilson Evans Batten Catalogue); b Barnes et al. (1986); c Nidever et al. (2002); d *ELODIE*; e De Medeiros & Major (1999); f Beavers et al. (1979); g Udry et al. (1999); h Benz & Major (1984); i Dyer (1954); j Soderblom (1982), Soderblom et al. (1989); k Fekel (1997); l De Medeiros et al. (2000); m Tokovinin (1992); n Marcy & Chen (1992).

Table A.2. Spectroscopic results of the sample. The stars marked with * in Col. 16 (MG) are inside the boundaries of the young disk population, but have high W velocities.

HD/ other name	ID	MJD (days)	Sp.T.	$B - V$ (mag)	V_r (km s ⁻¹)	\bar{V}_r (km s ⁻¹)	U (km s ⁻¹)	V (km s ⁻¹)	W (km s ⁻¹)	$v \sin i$ (km s ⁻¹)	$\overline{v \sin i}$ (km s ⁻¹)	P_{phot} (days)	$EW(\text{LiI})$ (mÅ)	$\overline{EW(\text{LiI})}$ (mÅ)	MG ^a
166	(5)	51 855.026	K0 V	0.75	...	-6.9 ± 0.1	-15.00	-21.60	-10.04	6.54 ± 1.00	6.54 ± 1.00	5.69	78.0 ± 0.5	75.5 ± 0.3	L A
	(5)	51 856.940			-6.94 ± 0.10					6.54 ± 1.00			73.0 ± 0.5		
1405	(1)	51 384.173	K2 V	1.04	-11.76 ± 0.59	-11.2 ± 0.1	-5.34	-28.85	-17.84	23.12 ± 1.60	23.88 ± 0.29	1.74	263.4 ± 1.7	268.2 ± 0.3	L A
	(1)	51 385.040			-11.49 ± 0.23					20.47 ± 2.07			256.4 ± 1.7		
	(1)	51 386.101			-12.50 ± 0.37					22.01 ± 1.39			265.4 ± 1.7		
	(1)	51 387.039			-10.51 ± 0.42					22.51 ± 1.47			263.4 ± 1.7		
	(1)	51 388.125			-11.95 ± 0.26					22.01 ± 1.32			250.4 ± 1.7		
	(1)	51 389.081			-11.11 ± 0.47					22.96 ± 1.43			269.4 ± 1.7		
	(2)	51 508.869			-9.41 ± 0.25					23.40 ± 1.00			278.4 ± 1.7		
	(2)	51 509.902			-10.28 ± 0.28					23.40 ± 1.00			273.4 ± 1.7		
	(4)	51 767.657			-10.52 ± 0.19					25.32 ± 1.90			294.4 ± 1.7		
	(4)	51 770.654			-10.40 ± 0.21					25.32 ± 1.90			314.4 ± 1.7		
	(5)	51 854.573			...					22.71 ± 1.90			247.4 ± 1.7		
	(5)	51 855.544			-11.47 ± 0.51					22.71 ± 1.90			256.4 ± 1.7		
	(5)	51 856.544			-10.50 ± 0.47					22.71 ± 1.90			266.4 ± 1.7		
	(5)	51 857.509			-10.98 ± 0.47					22.71 ± 1.90			272.4 ± 1.7		
	(7)	52 176.499			-10.66 ± 0.66					24.60 ± 0.84			271.4 ± 1.7		
	(7)	52 177.586			-12.53 ± 0.65					24.50 ± 0.91			273.4 ± 1.7		
	(9)	52 263.677			-13.08 ± 0.41					...			276.4 ± 1.7		
	(9)	52 264.654			-13.77 ± 0.30					...			283.4 ± 1.7		
	(9)	52 265.657			-12.45 ± 0.35					...			281.4 ± 1.7		
	(9)	52 266.668			-11.51 ± 0.34					...			269.4 ± 1.7		
	(9)	52 269.633			-12.40 ± 0.40					...			278.4 ± 1.7		
	(9)	52 270.632			-14.83 ± 0.35					...			268.4 ± 1.7		
	(9)	52 271.648			-12.34 ± 0.30					...			251.4 ± 1.7		
	(9)	52 272.626			-15.04 ± 0.46					...			264.4 ± 1.7		
	(9)	52 273.626			-11.90 ± 0.33					...			258.4 ± 1.7		
	(11)	52 457.112			-11.08 ± 0.51					25.17 ± 1.28			247.4 ± 1.7		
	(11)	52 458.104			-10.00 ± 0.54					26.38 ± 1.27			271.4 ± 1.7		
	(11)	52 459.117			-12.08 ± 0.42					24.73 ± 1.24			258.4 ± 1.7		
	(11)	52 460.090			-12.66 ± 0.46					25.61 ± 1.23			261.4 ± 1.7		
	(11)	52 462.091			-11.84 ± 0.39					23.78 ± 1.17			258.4 ± 1.7		
	(12)	52 508.686			-11.62 ± 0.28						
	(12)	52 509.692			-11.65 ± 0.34						
	(12)	52 510.700			-11.73 ± 0.25						
	(12)	52 511.586			-11.96 ± 0.33						
	(12)	52 512.725			-8.83 ± 0.26						
	(12)	52 512.737			-8.81 ± 0.32						
	(12)	52 513.719			-9.95 ± 0.29						
	(12)	52 514.687			-9.03 ± 0.40						
	(12)	52 515.615			-10.61 ± 0.34						
1326	(4)	51 769.185	M2 V	1.54	9.98 ± 0.29	10.8 ± 0.2	-48.71	-12.92	-3.16	7.95 ± 1.00	9.06 ± 0.79	YD
	(7)	52 177.039			11.39 ± 0.26					10.96 ± 1.31			
1835	(4)	51 769.169	G3 V	0.67	-4.50 ± 0.21	-1.8 ± 0.1	-35.78	-14.36	-0.96	7.26 ± 3.00	7.26 ± 3.00	7.65	79.0 ± 0.6	80.5 ± 0.4	HS
	(5)	51 855.982			-1.24 ± 0.10					...			82.0 ± 0.6		
2410	(4)	51 769.246	G7 III	0.99	3.66 ± 0.13	3.7 ± 0.1	-8.98	-5.33	-11.19	4.4 ± 0.6	4.4 ± 0.6	UMa
QT And	(8)	52 194.176	K2 V	0.92	5.32 ± 0.32	-8.98	-5.33	-11.19	-11.19	20.79 ± 1.03	20.79 ± 1.03	...	132.2 ± 4.5	132.2 ± 4.5	Ca

Table A.2. continued.

HD/ other name	ID	MJD (days)	Sp.T.	$B - V$ (mag)	V_r (km s ⁻¹)	\bar{V}_r (km s ⁻¹)	U (km s ⁻¹)	V (km s ⁻¹)	W (km s ⁻¹)	$v \sin i$ (km s ⁻¹)	$\overline{v \sin i}$ (km s ⁻¹)	P_{phot} (days)	$EW(\text{LiI})$ (mÅ)	$\overline{EW(\text{LiI})}$ (mÅ)	MG
	(6)	52 005.156			-8.79 ± 1.36					
	(10)	52 388.043			-3.43 ± 0.06					3.11 ± 0.68	93.5 ± 1.7	...	
115043	(3)	51 566.263	G2 V	0.61	-9.26 ± 0.29	-9.3 ± 0.3	14.52	2.19	-8.08	10.87 ± 0.86	10.87 ± 0.86	5.31	91.5 ± 0.5	91.5 ± 0.5	UMa
HIP 65016	(10)	52 388.010	M1.5 V	1.37	-10.76 ± 0.38	-10.8 ± 0.4	-12.79	-25.39	-6.76	2.90 ± 2.00	2.90 ± 2.00	LA
238224	(10)	52 389.082	K7 V	1.17	-9.75 ± 0.15	-9.7 ± 0.1	14.65	2.25	-8.86	6.82 ± 0.77	6.82 ± 0.77	UMa
117860	(6)	52 004.090	G0 -	0.63	-6.22 ± 7.67	-6.2 ± 7.7	-34.45	-14.52	5.20	HS
HIP 67092	(10)	52 388.992	K7 V	1.49	6.37 ± 0.15	-7.13	-22.99	3.33	LA
125161B	(10)	52 390.124	K1 V	0.62	-30.55 ± 0.13	-30.5 ± 0.1	-21.68	-21.20	-24.26	6.69 ± 0.98	6.69 ± 0.98	12.73	36.0 ± 1.3	36.0 ± 1.3	YD*
129333	(3)	51 563.305	G1.5 V	0.63	-19.37 ± 0.48	-20.6 ± 0.3	-7.25	-29.07	-4.65	19.68 ± 1.03	19.68 ± 1.03	2.79	187.9 ± 1.1	189.4 ± 0.8	LA
	(3)	51 566.310			-21.80 ± 0.46					19.68 ± 1.03	190.9 ± 1.1	...	
133826	(6)	52 003.119	G0 -	0.55	14.14 ± 6.64	14.1 ± 6.6	24.91	11.13	15.01	nYD
134319	(1)	51 384.846	G0 V	0.67	-6.45 ± 0.15	-6.5 ± 0.1	-32.45	-13.59	-2.82	11.60 ± 1.13	11.39 ± 0.66	4.45	148.2 ± 1.2	144.9 ± 0.7	HS
	(1)	51 388.845			-6.52 ± 0.27					11.23 ± 1.18	153.2 ± 1.2	...	
	(1)	51 388.831			-6.49 ± 0.14					11.34 ± 1.12	133.2 ± 1.2	...	
	(6)	52 003.183			
135363	(10)	52 389.068	K0 V	0.94	-5.61 ± 0.17	-5.6 ± 0.1	-26.74	-11.80	-8.61	18.97 ± 1.46	20.56 ± 0.46	...	193.3 ± 2.1	198.2 ± 0.8	HS
	(10)	52 390.110			-3.90 ± 0.15					18.46 ± 1.32	197.3 ± 2.1	...	
	(11)	52 457.900			-7.44 ± 0.27					21.91 ± 1.22	200.3 ± 2.1	...	
	(11)	52 458.907			-5.43 ± 0.21					20.77 ± 1.12	198.3 ± 2.1	...	
	(11)	52 459.876			-7.54 ± 0.23					21.39 ± 1.14	206.3 ± 2.1	...	
	(11)	52 460.894			-4.75 ± 0.27					20.37 ± 1.11	196.3 ± 2.1	...	
	(11)	52 461.878			-7.33 ± 0.23					21.09 ± 1.17	195.3 ± 2.1	...	
140913	(11)	52 459.147	G5 V	0.61	-20.30 ± 0.09	-20.3 ± 0.1	-24.29	-16.98	-2.88	8.44 ± 0.85	8.44 ± 0.85	6.13	75.6 ± 0.6	75.6 ± 0.6	IC
142764	(6)	52 002.172	K5 III	1.83	...	-56.4 ± 0.1	-39.09	-15.32	-37.68	...	1.00 ± 1.00	nYD
	(6)	52 003.247			
	(10)	52 390.095			-56.50 ± 0.11					1.00 ± 1.00	
143809	(11)	52 458.955	G5 V	0.55	-9.12 ± 0.15	-9.1 ± 0.1	-5.34	-24.97	-0.42	16.45 ± 1.51	16.45 ± 1.51	...	103.0 ± 1.9	103.0 ± 1.9	LA
145675	(11)	52 458.982	K2 IV	0.89	-13.93 ± 0.08	-13.9 ± 0.1	23.74	-12.34	-16.14	1.00 ± 1.00	1.00 ± 1.00	50.68	9.4 ± 0.5	9.4 ± 0.5	nYD
146696	(6)	52 002.215	G0 -	0.64	12.83 ± 8.49	12.8 ± 8.5	30.24	16.51	-7.18	nYD
147379A	(4)	51 767.969	K7 V	1.34	-16.25 ± 0.45	-17.8 ± 0.1	-9.86	-28.97	4.60	14.85 ± 1.00	9.69 ± 0.52	LA
	(10)	52 388.057			-17.86 ± 0.20					8.66 ± 0.88	
	(10)	52 389.127			-17.95 ± 0.20					7.00 ± 0.84	
147379B	(10)	52 388.072	M3 V	1.22	-17.50 ± 0.63	-17.5 ± 0.6	-10.07	-28.27	4.19	2.90 ± 2.00	2.90 ± 2.00	LA
HIP 79796	(11)	52 457.916	M1 V	1.24	-28.25 ± 0.71	-28.7 ± 0.3	41.76	-28.59	-15.63	17.60 ± 1.22	17.36 ± 0.55	nYD
	(11)	52 458.890			-29.10 ± 0.61					15.77 ± 1.68	
	(11)	52 459.905			-28.46 ± 0.68					16.93 ± 1.14	
	(11)	52 460.910			-29.75 ± 0.85					18.45 ± 1.15	
	(11)	52 461.894			-28.22 ± 0.69					17.25 ± 1.17	
149661	(4)	51 766.930	G9 V	0.84	-12.80 ± 0.07	-12.8 ± 0.1	0.98	-0.39	-28.49	7.94 ± 1.90	7.94 ± 1.90	11.00	32.2 ± 0.4	32.2 ± 0.4	YD*
149931	(6)	52 002.263	F5 -	0.74	-12.52 ± 4.53	-12.5 ± 4.5	16.20	-22.42	-13.66	nYD
152863	(11)	52 459.933	K0 III	0.93	-0.37 ± 0.06	-0.4 ± 0.1	12.46	0.50	-13.03	4.84 ± 0.75	4.84 ± 0.75	UMa
152751	(4)	51 767.922	M3.5 V	1.49	...	19.8 ± 0.8	22.57	-28.65	11.80	...	2.90 ± 2.00	nYD
	(4)	51 767.937			
	(4)	51 767.952			
	(4)	51 768.897			
	(4)	51 768.912			
	(4)	51 768.927			
	(4)	51 768.942			

Table A.2. continued.

HD/ other name	ID	MJD (days)	Sp.T.	$B - V$ (mag)	V_r (km s ⁻¹)	\bar{V}_r (km s ⁻¹)	U (km s ⁻¹)	V (km s ⁻¹)	W (km s ⁻¹)	$v \sin i$ (km s ⁻¹)	$\overline{v \sin i}$ (km s ⁻¹)	P_{phot} (days)	$EW(\text{LiI})$ (mÅ)	$EW(\text{LiI})$ (mÅ)	MG
	(4)	51 769.876							
	(4)	51 769.971							
	(10)	52 388.121			19.84 ± 0.80					2.90 ± 2.00					
155674A	(10)	52 389.157	K5 V	1.19	4.49 ± 0.12	4.5 ± 0.1	12.67	6.52	-3.50	4.23 ± 1.07	4.23 ± 1.07	...			UMa
155674B	(10)	52 389.169	K7 V	1.22	3.66 ± 0.14	3.7 ± 0.1	11.91	6.18	-4.26	1.40 ± 1.00	1.40 ± 1.00	...			UMa
156984	(6)	52 004.211	K0 -	1.24	-96.85 ± 2.38	-96.8 ± 2.4			nYD
HIP 84794	(11)	52 458.993	M3.5 V	1.46	...	-35.7 ± 1.0	-37.65	-19.97	-3.08	1.00 ± 1.00	1.00 ± 1.00	...			HS
	(11)	52 459.016			...					1.00 ± 1.00					
HIP 85665	(11)	52 457.941	M1 V	1.37	-35.70 ± 1.06	-13.1 ± 0.3	-3.99	-13.50	-10.74	7.40 ± 0.84	7.40 ± 0.84	...			LA
160934	(4)	51 767.988	K7 V	1.30	-31.54 ± 0.34	-38.2 ± 0.1	-5.03	-33.61	-18.36	19.73 ± 1.00	19.07 ± 0.38	1.84	9.1 ± 8.6	3.8 ± 3.2	LA
	(10)	52 388.092			-39.76 ± 0.34				18.58 ± 0.99				2.1 ± 8.6		
	(10)	52 389.139			-40.56 ± 0.32				19.73 ± 1.02				4.1 ± 8.6		
	(10)	52 390.137			-40.64 ± 0.35				19.97 ± 1.03				7.1 ± 8.6		
	(11)	52 459.939			-38.66 ± 0.44				18.31 ± 0.97				0.1 ± 8.6		
	(11)	52 460.941			-38.37 ± 0.42				18.53 ± 0.97				...		
	(11)	52 462.046			-38.25 ± 0.46				18.83 ± 0.98				4.1 ± 8.6		
162283	(10)	52 390.166	M0 V	1.66	-24.80 ± 0.20	-24.8 ± 0.2	-17.49	-20.57	-8.88	10.98 ± 0.43	10.98 ± 0.43	...			LA
HIP 87579	(11)	52 457.967	K3 V	0.95	-13.28 ± 0.06	-13.3 ± 0.1	-13.41	-9.59	4.60	7.98 ± 0.67	7.71 ± 0.51	...			Ca
	(11)	52 460.928			-13.27 ± 0.12				7.33 ± 0.80				...		
HIP 87768	(11)	52 461.923	K5 V	1.09	-30.05 ± 0.15	-30.0 ± 0.2	-16.23	-25.00	-8.00	6.92 ± 0.77	6.92 ± 0.77	...			LA
GJ 698B	(11)	52 461.937	M3 V	1.46	-30.07 ± 0.68	-30.1 ± 0.7	-16.30	-25.06	-8.04	7.67 ± 0.90	7.67 ± 0.90	...			LA
165341	(4)	51 768.966	K0 V	0.83	-4.07 ± 0.17	-4.1 ± 0.2	9.74	-17.90	-18.41	19.70	12.6 ± 1.1	12.6 ± 1.1	YD
GJ 702B	(4)	51 768.973	K5 V	0.83	-6.48 ± 0.13	-6.5 ± 0.1	9.43	-19.99	-24.11	YD
167605	(4)	51 766.947	K2 V	0.94	-13.79 ± 0.09	-13.7 ± 0.1	-25.39	-18.68	-2.98	11.98 ± 1.90	11.98 ± 1.90	...	21.4 ± 2.0	21.9 ± 1.4	IC
	(4)	51 770.014			-13.69 ± 0.09				11.98 ± 1.90			...	22.4 ± 2.0		
234601	(11)	52 457.980	G5 V	0.65	-17.91 ± 0.09	-17.9 ± 0.1	-19.74	-17.44	2.44	8.09 ± 1.13	8.09 ± 1.13	7.35	87.1 ± 1.9	87.1 ± 1.9	IC
SAO 9067	(10)	52 389.098	G5 V	0.80	-1.26 ± 0.08	-1.3 ± 0.1	-4.73	-1.72	-1.32	11.40 ± 0.82	11.40 ± 0.82	...	79.8 ± 4.3	79.8 ± 4.3	YD
168442	(11)	52 461.960	K7 V	1.40	-14.64 ± 0.20	-14.6 ± 0.2	-12.93	-6.60	-1.55	6.42 ± 0.78	6.42 ± 0.78	Ca
HIP 89874	(4)	51 769.935	K5 V	1.62	-9.69 ± 0.25	-9.7 ± 0.2	-4.42	-14.69	-12.26	20.08 ± 1.00	20.08 ± 1.00	5.15	550.4 ± 24	555.4 ± 17	LA
	(4)	51 769.954			560.4 ± 24		
171488	(4)	51 768.956	G2 V	0.62	-19.66 ± 0.46	-21.6 ± 0.3	-6.90	-22.10	-4.96	45.20 ± 3.00	42.16 ± 1.31	1.34	220.4 ± 0.8	208.4 ± 0.6	LA
	(6)	52 005.227			-16.84 ± 2.33				
	(7)	52 175.845			-23.62 ± 0.44				41.45 ± 1.45			...	196.4 ± 0.8		
171746	(7)	52 174.827	G2 V	0.55	8.47 ± 0.07	8.5 ± 0.1	11.96	3.30	-10.12	10.37 ± 0.82	10.37 ± 0.82	...	58.9 ± 1.0	58.9 ± 1.0	UMa
173739	(4)	51 768.987	M3 V	1.45	-1.06 ± 0.46	-1.0 ± 0.5	-25.48	-12.42	25.86	7.72 ± 1.00	7.72 ± 1.00	YD*
	(4)	51 769.894			
173740	(6)	52 005.231			YD*
	(4)	51 769.005	M3.5 V	1.53	0.42 ± 0.49	0.4 ± 0.5	-25.00	-11.41	27.01	1.60 ± 1.00	1.60 ± 1.00	YD*
	(4)	51 769.912			
2RE J1846+191	(11)	52 460.979	K4 V	1.49	-10.37 ± 0.73	-10.4 ± 0.5	6.28	-13.78	-23.99	27.81 ± 1.47	25.54 ± 0.95	YD
	(11)	52 461.998			-10.51 ± 0.65				23.89 ± 1.25			
GJ 734B	(11)	52 459.988	M3.5 V	1.42	-26.17 ± 0.99	-26.2 ± 1.0	-25.72	-11.16	1.79	1.40 ± 1.00	1.40 ± 1.00	HS
184525	(11)	52 460.077	G5 V	0.63	0.81 ± 0.08	0.8 ± 0.1	20.99	-17.71	1.84	9.54 ± 0.89	9.54 ± 0.89	nYD
187458	(11)	52 459.147	F5/6 V	0.44	-26.20 ± 0.33	-26.2 ± 0.3	-35.84	-14.06	-12.34	15.61 ± 1.55	15.61 ± 1.55	HS
187565	(7)	52 176.839	F8 V	0.49	-26.34 ± 0.18	-26.3 ± 0.2	-31.81	-14.08	-8.68	17.43 ± 0.87	17.43 ± 0.87	...	4.3 ± 0.8	4.3 ± 0.8	HS
191011	(7)	52 175.855	K3 III	1.68	22.85 ± 0.10	23.1 ± 0.1	10.29	20.26	-5.44	3.00 ± 2.00	2.83 ± 0.59	20.20	nYD
	(10)	52 388.180			24.26 ± 0.18				1.40 ± 1.00			

Table A.2. continued.

HD/ other name	ID	MJD (days)	Sp.T.	$B - V$ (mag)	V_r (km s ⁻¹)	\bar{V}_r (km s ⁻¹)	U (km s ⁻¹)	V (km s ⁻¹)	W (km s ⁻¹)	$v \sin i$ (km s ⁻¹)	$\overline{v \sin i}$ (km s ⁻¹)	P_{phot} (days)	$EW(\text{LiI})$ (mÅ)	$\overline{EW(\text{LiI})}$ (mÅ)	MG
GJ 856B	(8)	52 194.123	M1 V	1.49	-21.74 ± 1.08	-21.7 ± 1.0	-6.62	-28.79	-28.79	17.72 ± 1.89	17.72 ± 1.89	YD*
213845	(4)	51 768.084	F7 V	0.45	-0.54 ± 0.36	-0.5 ± 0.4	-14.49	-20.17	-14.12	41.20 ± 0.70	41.20 ± 0.70	LA
BD+17 4799	(4)	51 767.095	K0 V/IV	0.88	-16.77 ± 0.12	-16.4 ± 0.5	-6.26	-24.73	-7.06	14.72 ± 1.00	11.03 ± 0.38	...	262.9 ± 3.2	247.6 ± 1.6	LA
	(5)	51 855.923			10.96 ± 1.00	256.9 ± 3.2	...	LA
	(7)	52 175.979			-16.56 ± 0.06	9.45 ± 0.67	239.9 ± 3.2	...	LA
	(11)	52 460.110			-14.21 ± 0.17	10.98 ± 0.63	230.9 ± 3.2	...	LA
HIP 112460	(4)	51 768.119	M3.5 V	1.39	0.87 ± 0.94	0.6 ± 0.3	19.71	3.89	-1.82	1.36 ± 1.00	2.01 ± 0.53	4.38	UMa
	(4)	51 769.129			1.36 ± 1.00	UMa
	(4)	51 770.118			1.36 ± 1.00	UMa
	(7)	52 176.016			UMa
	(7)	52 176.990			UMa
	(8)	52 194.012			0.61 ± 0.36	UMa
216899	(7)	52 174.966	M1.5 V	1.40	-27.70 ± 0.20	-27.7 ± 0.2	32.50	-16.93	25.42	9.68 ± 0.84	9.68 ± 0.84	...	2.9 ± 3.2	2.9 ± 3.2	nYD
217813	(5)	51 854.943	G1 V	0.62	1.22 ± 0.08	1.2 ± 0.1	13.14	3.60	2.51	5.08 ± 3.00	5.08 ± 3.00	8.10	94.3 ± 1.0	94.3 ± 1.0	UMa
HIP 114066	(8)	52 194.063	M0 V	1.21	-22.85 ± 0.22	-22.8 ± 0.2	-7.11	-26.39	-15.94	8.05 ± 0.82	8.05 ± 0.82	...	14.6 ± 13.5	14.6 ± 13.5	LA
220140	(1)	51 384.042	K0 V	0.89	-16.41 ± 0.39	-16.3 ± 0.1	-10.35	-23.14	-5.33	16.78 ± 1.21	16.78 ± 0.39	2.74	208.3 ± 0.8	205.3 ± 0.2	LA
	(1)	51 385.008			-17.02 ± 0.19	201.3 ± 0.8	...	LA
	(1)	51 386.172			-16.58 ± 0.24	16.66 ± 1.20	210.3 ± 0.8	...	LA
	(1)	51 387.093			-16.83 ± 0.32	16.15 ± 1.14	204.3 ± 0.8	...	LA
	(1)	51 388.034			-16.74 ± 0.32	16.49 ± 1.16	188.3 ± 0.8	...	LA
	(1)	51 389.029			-16.50 ± 0.32	15.15 ± 1.18	205.3 ± 0.8	...	LA
	(2)	51 509.874			-15.72 ± 0.38	16.10 ± 1.00	199.3 ± 0.8	...	LA
	(5)	51 854.912			-16.30 ± 0.11	18.88 ± 1.90	215.3 ± 0.8	...	LA
	(5)	51 856.918			-16.62 ± 0.13	18.88 ± 1.90	206.3 ± 0.8	...	LA
	(5)	51 857.922			-15.75 ± 0.09	18.88 ± 1.90	219.3 ± 0.8	...	LA
	(7)	52 175.966			-16.57 ± 0.10	17.97 ± 0.76	201.3 ± 0.8	...	LA
221503	(4)	51 768.164	M0 V	1.25	0.59 ± 0.10	0.3 ± 0.1	-13.29	-21.22	-9.87	...	7.47 ± 1.00	LA
	(5)	51 855.939			-0.90 ± 0.22	7.47 ± 1.00	LA
HIP 117779	(7)	52 176.976	K5 V	1.39	2.04 ± 0.11	2.0 ± 0.1	5.42	5.88	2.50	UMa
HIP 118212	(8)	52 194.080	M0 V	1.35	6.74 ± 0.15	6.7 ± 0.1	-48.96	-17.65	-12.92	1.40 ± 1.00	1.40 ± 1.00	HS

Notes. ^(c) LA: Local Association, HS: Hyades Supercluster, UMa: Ursa Major Moving Group, IC: IC 2391 Supercluster, Ca: Castor Moving Group, YD: other Young Disk star, and nYD: not Young Disk star.

Table A.3. continued.

HD/ other name	ID	MJD (days)	$EW(\text{\AA})$ in the subtracted spectrum															
			Ca II			H			He I			Na I			Ca II IRT			
			K	H	He I	H δ	H γ	H β	D ₃	D ₂	D ₁	H α	λ 8498	λ 8542	λ 8662			
	(5)	51 853.9877	1.04 ± 0.19	0.26 ± 0.04	0.74 ± 0.11	0.39 ± 0.04	0.64 ± 0.07	...			
	(5)	51 854.8790	0.96 ± 0.10	0.16 ± 0.03	0.59 ± 0.05	0.39 ± 0.06	0.58 ± 0.10	...			
	(5)	51 855.8679	0.89 ± 0.23	0.35 ± 0.08	0.69 ± 0.13	0.47 ± 0.05	0.64 ± 0.09	...			
	(5)	51 856.8901	0.56 ± 0.11	0.16 ± 0.04	0.51 ± 0.06	0.35 ± 0.06	0.55 ± 0.09	...			
	(5)	51 857.9473	0.17 ± 0.07	0.59 ± 0.10	0.39 ± 0.05	0.63 ± 0.09	...			
GJ 856B	(7)	52 174.9359	0.98 ± 0.15	0.75 ± 0.10	0.31 ± 0.19	0.36 ± 0.10	0.23 ± 0.03	0.49 ± 0.03	0.35 ± 0.03	4.10 ± 0.24	0.44 ± 0.06	0.68 ± 0.04	0.56 ± 0.03			
213845	(8)	52 194.1237	0.35 ± 0.08			
BD+17 4799	(4)	51 768.0842			
	(4)	51 767.0955	0.16 ± 0.04	0.51 ± 0.08	0.40 ± 0.04	0.61 ± 0.06	0.53 ± 0.07			
	(5)	51 855.9232	0.91 ± 0.02	0.18 ± 0.10	0.76 ± 0.11	0.45 ± 0.07	0.56 ± 0.12	...			
	(7)	52 175.9793	0.77 ± 0.18	0.70 ± 0.06	0.21 ± 0.06	...	0.03 ± 0.04	0.09 ± 0.06	0.51 ± 0.04	0.38 ± 0.04	0.46 ± 0.06	0.48 ± 0.04			
	(11)	52 460.1102	0.87 ± 0.06	0.56 ± 0.03	0.11 ± 0.05	0.06 ± 0.04	0.04 ± 0.03	0.24 ± 0.04	0.67 ± 0.06	0.27 ± 0.02	0.41 ± 0.05	0.34 ± 0.02			
HIP 112460	(4)	51 768.1192			
	(4)	51 769.1298			
	(4)	51 770.1180			
	(7)	52 176.0162	...	7.61 ± 0.09	4.12 ± 0.11	4.08 ± 0.16	5.23 ± 0.08	4.48 ± 0.18	0.40 ± 0.06	0.32 ± 0.03	0.22 ± 0.03	4.40 ± 0.23	0.40 ± 0.05	0.85 ± 0.08	0.41 ± 0.06			
	(7)	52 176.9905	5.83 ± 0.17	5.05 ± 0.12	3.17 ± 0.15	5.29 ± 0.47	6.57 ± 0.24	5.70 ± 0.21	0.56 ± 0.06	0.38 ± 0.05	0.29 ± 0.05	5.25 ± 0.24	0.47 ± 0.05	0.93 ± 0.08	0.46 ± 0.06			
216899	(8)	52 194.0121	0.34 ± 0.05	0.31 ± 0.02	0.21 ± 0.02	3.81 ± 0.12	0.30 ± 0.08	0.45 ± 0.11	0.19 ± 0.10			
217813	(7)	52 174.9664	1.63 ± 0.18	1.09 ± 0.09	0.11 ± 0.04	0.13 ± 0.03	0.30 ± 0.05	0.25 ± 0.03			
HIP 114066	(5)	51 854.9430	0.18 ± 0.05	0.08 ± 0.02	0.08 ± 0.03	0.20 ± 0.08	...			
220140	(8)	52 194.0639	0.08 ± 0.04	0.12 ± 0.02	0.07 ± 0.02	2.06 ± 0.11	0.40 ± 0.06	0.58 ± 0.07	0.43 ± 0.14			
	(1)	51 384.0420	1.25 ± 0.08	0.68 ± 0.03	0.20 ± 0.04	0.17 ± 0.09	0.22 ± 0.04	0.28 ± 0.05	0.82 ± 0.08	0.36 ± 0.04	0.48 ± 0.06	0.40 ± 0.03			
	(1)	51 385.0085	...	0.65 ± 0.05	0.25 ± 0.07	0.14 ± 0.09	0.16 ± 0.04	0.27 ± 0.06	0.77 ± 0.08	0.36 ± 0.05	0.48 ± 0.07	0.40 ± 0.06			
	(1)	51 386.1725	0.87 ± 0.22	0.59 ± 0.09	0.20 ± 0.14	0.17 ± 0.10	0.14 ± 0.03	0.23 ± 0.08	0.85 ± 0.05	0.34 ± 0.05	0.48 ± 0.08	0.40 ± 0.06			
	(1)	51 387.0935	0.97 ± 0.09	0.61 ± 0.04	0.19 ± 0.06	0.20 ± 0.09	0.18 ± 0.04	0.27 ± 0.04	1.00 ± 0.08	0.37 ± 0.04	0.49 ± 0.05	0.42 ± 0.04			
	(1)	51 388.0347	0.93 ± 0.08	0.65 ± 0.05	0.23 ± 0.09	0.08 ± 0.05	0.08 ± 0.03	0.28 ± 0.04	0.64 ± 0.08	0.32 ± 0.05	0.43 ± 0.07	0.39 ± 0.05			
	(1)	51 389.0296	1.23 ± 0.07	0.78 ± 0.06	0.29 ± 0.14	0.46 ± 0.10	1.11 ± 0.14	0.39 ± 0.08	0.52 ± 0.12	0.52 ± 0.07			
	(2)	51 509.8749	1.07 ± 0.12	0.22 ± 0.15	0.55 ± 0.09	0.31 ± 0.07	0.65 ± 0.09	...			
	(5)	51 854.9124	0.98 ± 0.08	0.20 ± 0.07	0.06 ± 0.07	0.31 ± 0.08	0.68 ± 0.05	0.37 ± 0.09	0.56 ± 0.14	...			
	(5)	51 856.9186	0.48 ± 0.11	0.05 ± 0.06	0.17 ± 0.05	0.55 ± 0.04	0.31 ± 0.04	0.38 ± 0.06	...			
	(5)	51 857.9228	0.98 ± 0.13	0.29 ± 0.08	0.64 ± 0.07	0.30 ± 0.06	0.31 ± 0.18	...			
	(7)	52 175.9666	1.06 ± 0.08	0.58 ± 0.04	0.14 ± 0.05	0.11 ± 0.07	0.12 ± 0.04	0.25 ± 0.04	0.67 ± 0.06	0.38 ± 0.04	0.55 ± 0.06	0.48 ± 0.03			
221503	(4)	51 768.1646	0.12 ± 0.04	...	0.36 ± 0.08	0.23 ± 0.06			
	(5)	51 855.9396	0.16 ± 0.03	0.11 ± 0.04	0.25 ± 0.07	...			
HIP 117779	(7)	52 176.9769	1.72 ± 0.09	1.51 ± 0.08	0.33 ± 0.12	0.12 ± 0.04	0.04 ± 0.05	0.04 ± 0.02	0.05 ± 0.01			
HIP 118212	(8)	52 194.0805	0.10 ± 0.02	0.06 ± 0.07	0.10 ± 0.05	...			

Table A.4. continued.

HD/ other name	ID	MJD (days)	Ca II		H		He		H δ		H γ		H β		He I		Na I		H α	Ca II IRT		R'_{HK}
			K	H	H ϵ	H δ	H γ	H β	D ₃	D ₂	D ₁	λ 8498	λ 8542	λ 8662								
213845	(4)	51 768.0842
BD+17 4799	(4)	51 767.0955
	(5)	51 855.9232	6.43 \pm 0.02
(7)	(7)	52 175.9793	6.36 \pm 0.23	6.32 \pm 0.09	5.79 \pm 0.29
	(11)	52 460.1102	6.41 \pm 0.07	6.22 \pm 0.05	5.51 \pm 0.45	5.26 \pm 0.67	5.09 \pm 0.75	5.89 \pm 0.17
HIP 112460	(4)	51 768.1192
	(4)	51 769.1298
(7)	(4)	51 770.1180
	(7)	52 176.0162	...	6.33 \pm 0.01	6.07 \pm 0.03	6.09 \pm 0.04	6.26 \pm 0.02	6.31 \pm 0.04	5.49 \pm 0.15	5.39 \pm 0.09	5.23 \pm 0.14	6.68 \pm 0.05	5.73 \pm 0.12	6.06 \pm 0.09	5.75 \pm 0.15
(7)	(7)	52 176.9905	6.22 \pm 0.03	6.16 \pm 0.02	5.95 \pm 0.05	6.21 \pm 0.09	6.35 \pm 0.04	6.41 \pm 0.04	5.63 \pm 0.11	5.46 \pm 0.13	5.35 \pm 0.17	6.76 \pm 0.05	5.80 \pm 0.11	6.10 \pm 0.09	5.79 \pm 0.13
	(8)	52 194.0121
216899	(7)	52 174.9664	5.63 \pm 0.11	5.46 \pm 0.08
217813	(5)	51 854.9430	6.24 \pm 0.28
HIP 114066	(8)	52 194.0639
	(1)	51 384.0420	6.54 \pm 0.06	6.27 \pm 0.04	5.74 \pm 0.20	5.68 \pm 0.53	5.80 \pm 0.18	5.93 \pm 0.18	5.02 \pm 0.50	5.20 \pm 0.17	4.97 \pm 0.29	6.54 \pm 0.05	5.86 \pm 0.15	6.02 \pm 0.12	5.89 \pm 0.33
220140	(1)	51 385.0085	...	6.25 \pm 0.08	5.84 \pm 0.28	5.59 \pm 0.64	5.66 \pm 0.25	5.92 \pm 0.22
	(1)	51 386.1725	6.38 \pm 0.25	6.21 \pm 0.15	5.74 \pm 0.70	5.68 \pm 0.59	5.61 \pm 0.21	5.85 \pm 0.35
(1)	(1)	51 387.0935	6.43 \pm 0.09	6.23 \pm 0.07	5.72 \pm 0.32	5.75 \pm 0.45	5.72 \pm 0.22	5.92 \pm 0.15
	(1)	51 388.0347	6.41 \pm 0.09	6.25 \pm 0.08	5.80 \pm 0.39	5.35 \pm 0.62	5.36 \pm 0.38	5.93 \pm 0.14
(1)	(1)	51 389.0296	6.53 \pm 0.06	6.33 \pm 0.08	5.90 \pm 0.48	6.15 \pm 0.22
	(2)	51 509.8749	6.47 \pm 0.11	5.83 \pm 0.68
(5)	(5)	51 854.9124	6.43 \pm 0.08	5.75 \pm 0.35	5.24 \pm 1.17	5.98 \pm 0.26
	(5)	51 856.9186	6.12 \pm 0.23	5.16 \pm 1.20	5.72 \pm 0.29
(5)	(5)	51 857.9228	6.43 \pm 0.13	5.95 \pm 0.28
	(7)	52 175.9666	6.47 \pm 0.08	6.20 \pm 0.07	5.59 \pm 0.36	5.49 \pm 0.64	5.54 \pm 0.33	5.89 \pm 0.16
221503	(4)	51 768.1646
HIP 117779	(5)	51 855.9396
	(7)	52 176.9769	5.68 \pm 0.05	5.62 \pm 0.05	4.96 \pm 0.36
HIP 118212	(8)	52 194.0805

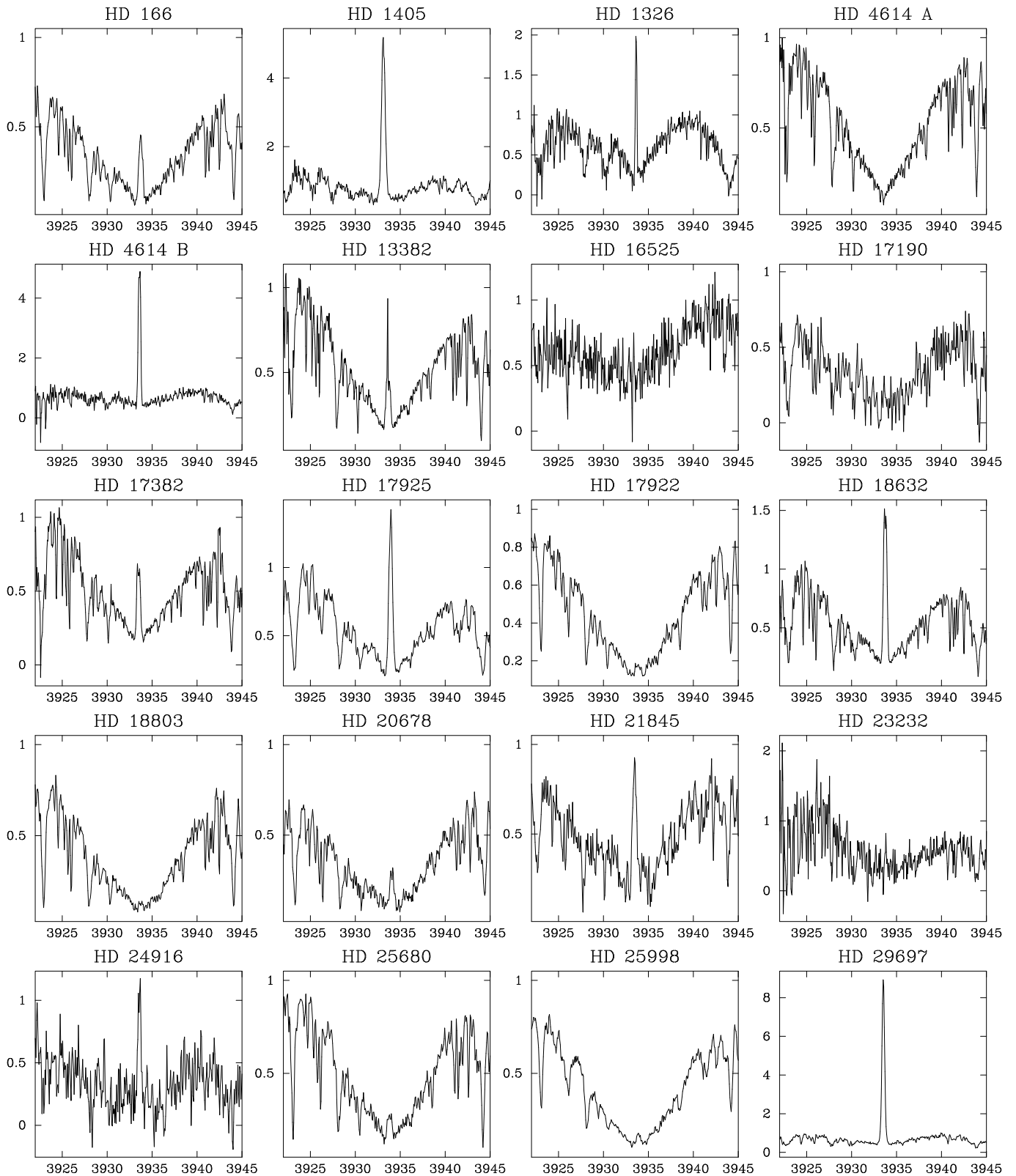


Fig. A.1. Ca II K spectra of the stars of our sample with observations in the H & K wavelength range.

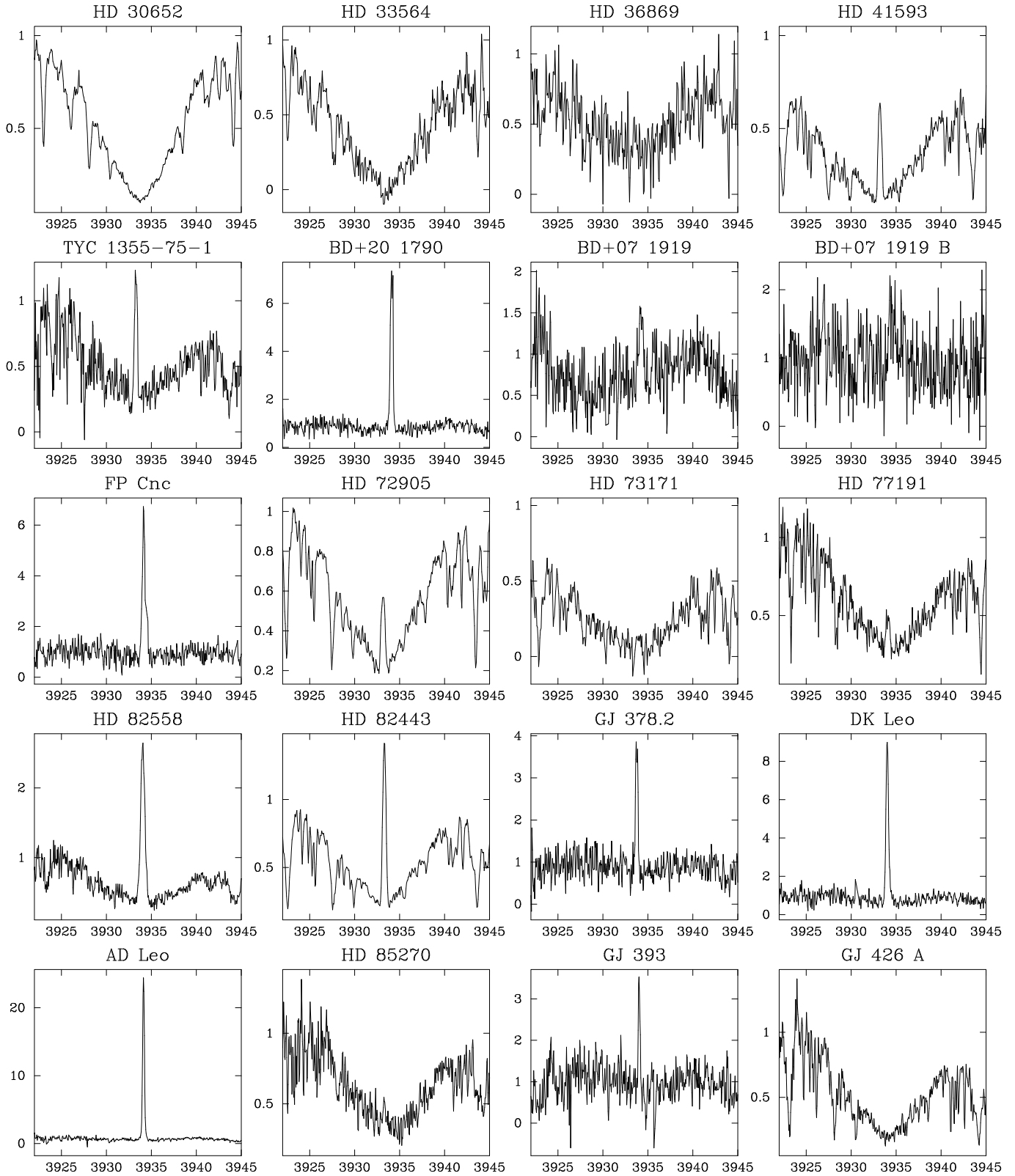


Fig. A.1. continued.

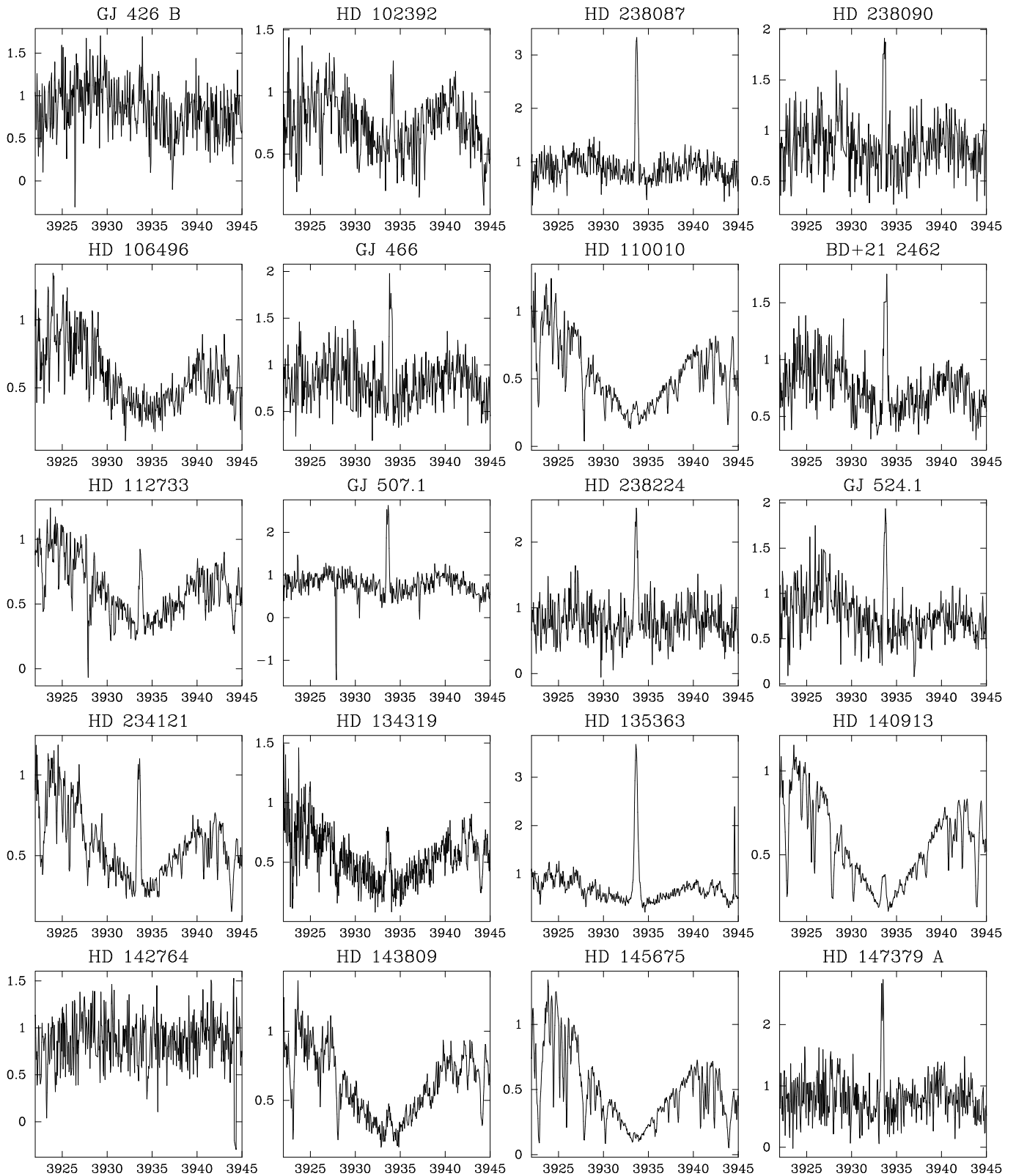


Fig. A.1. continued.

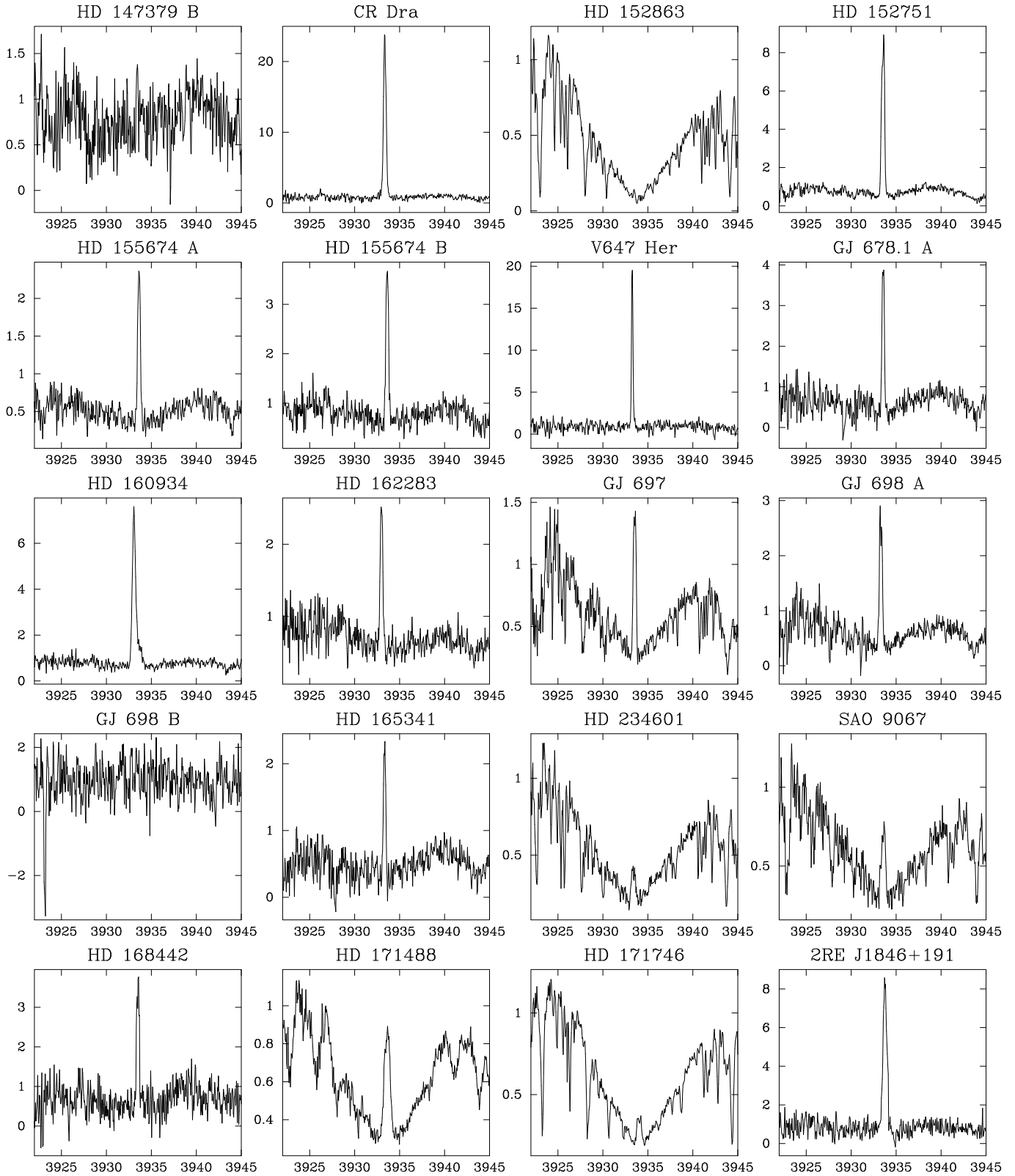


Fig. A.1. continued.

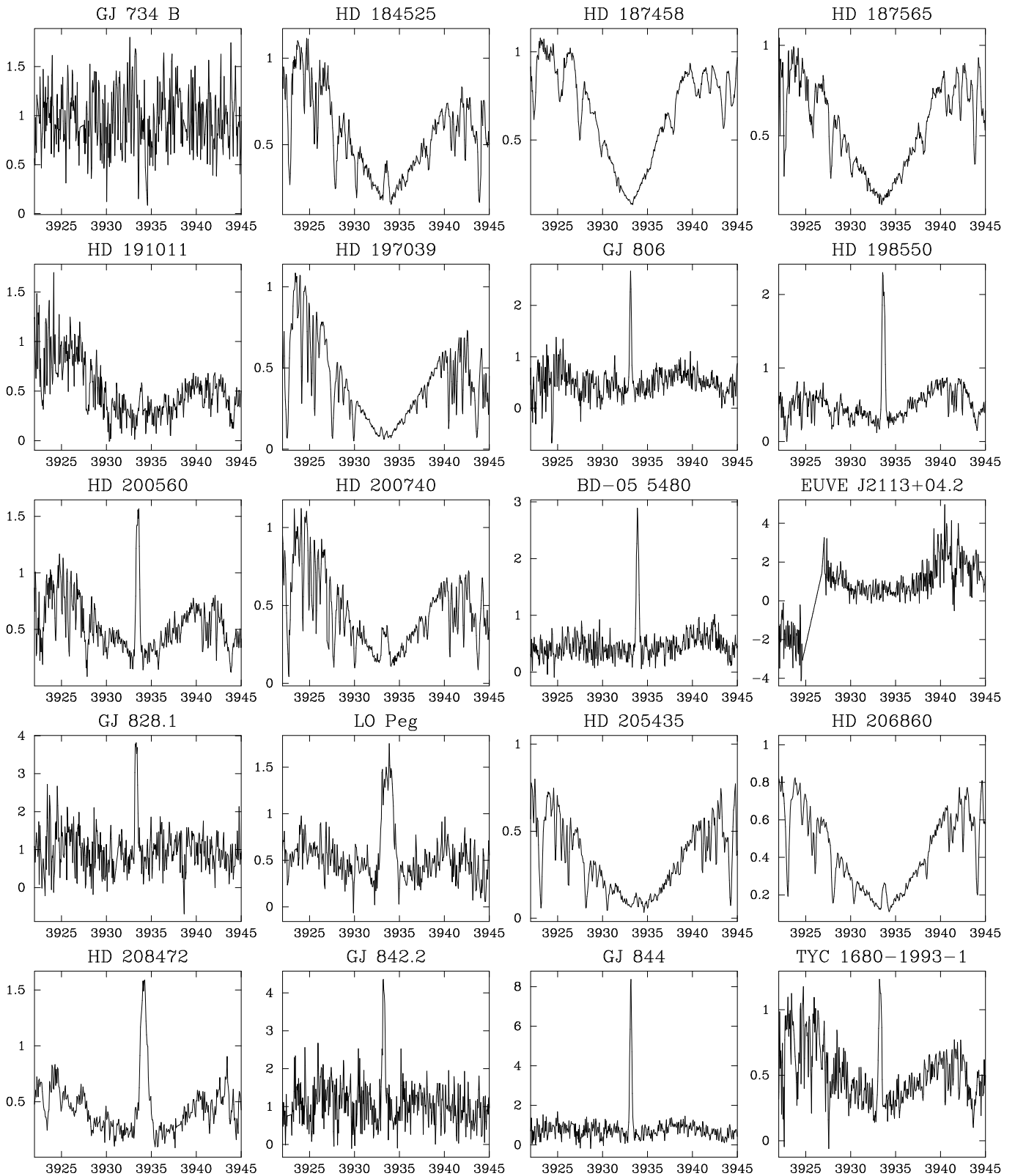


Fig. A.1. continued.

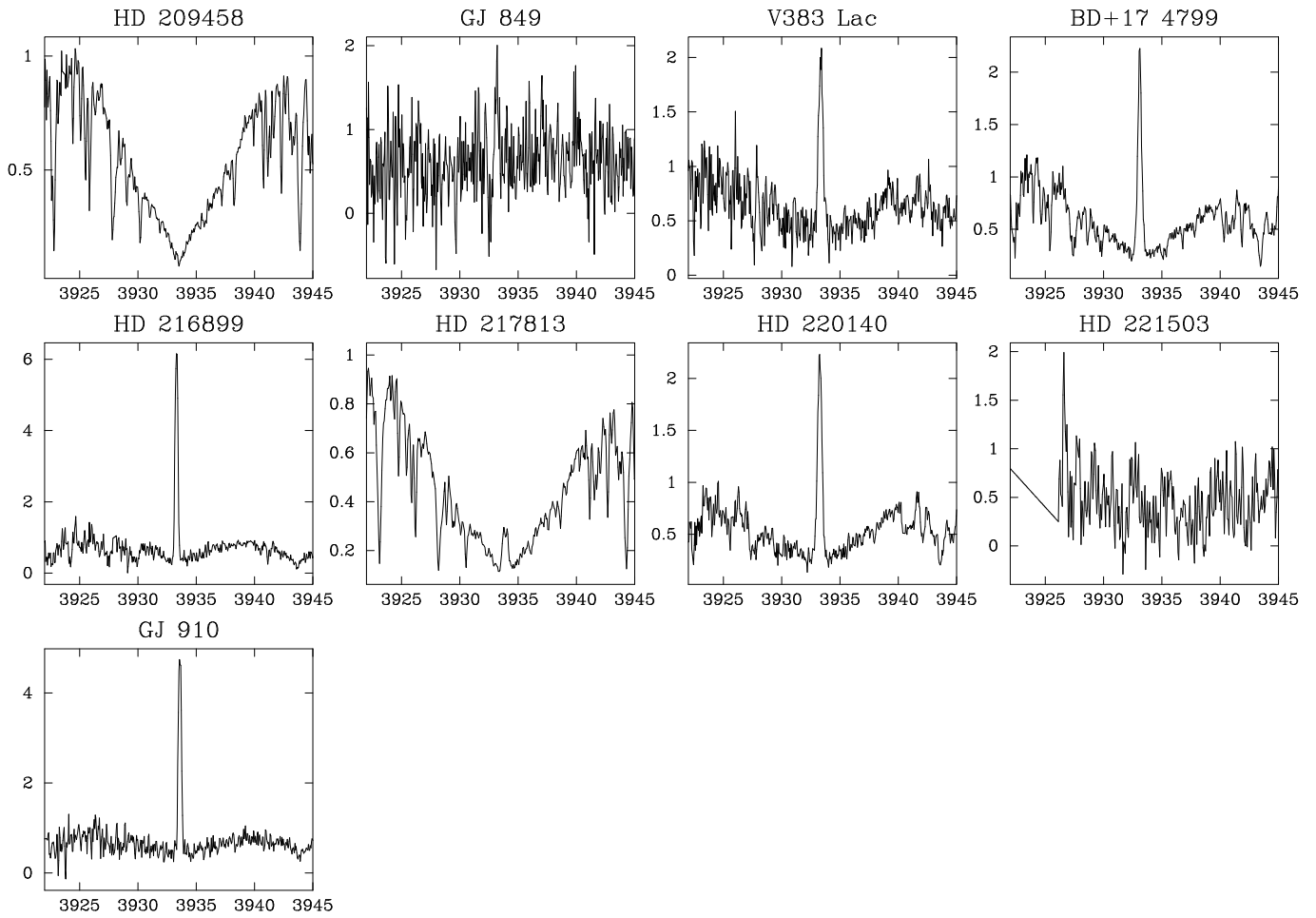


Fig. A.1. continued.

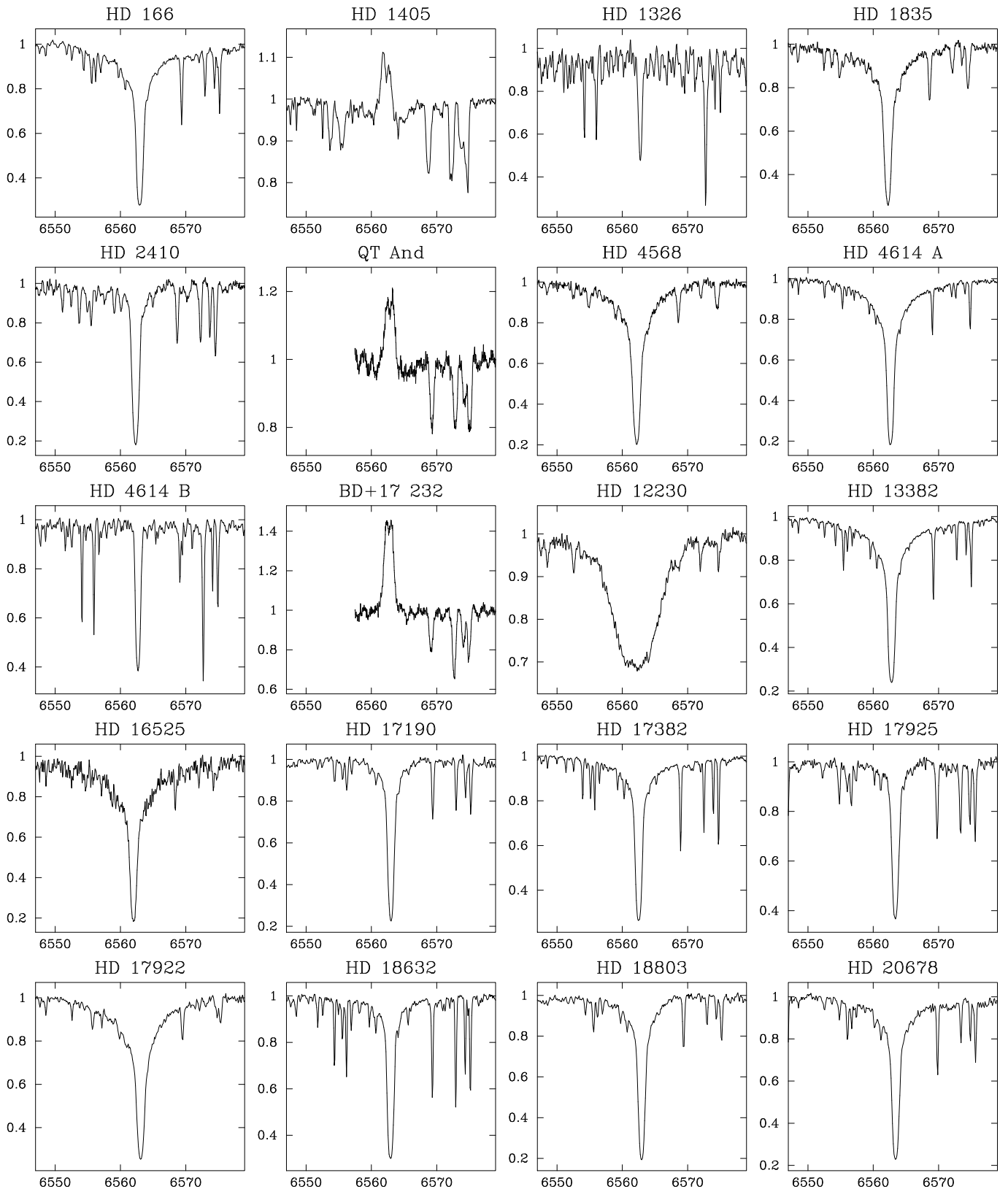


Fig. A.2. H α spectra of the stars of our sample with observations in H α .

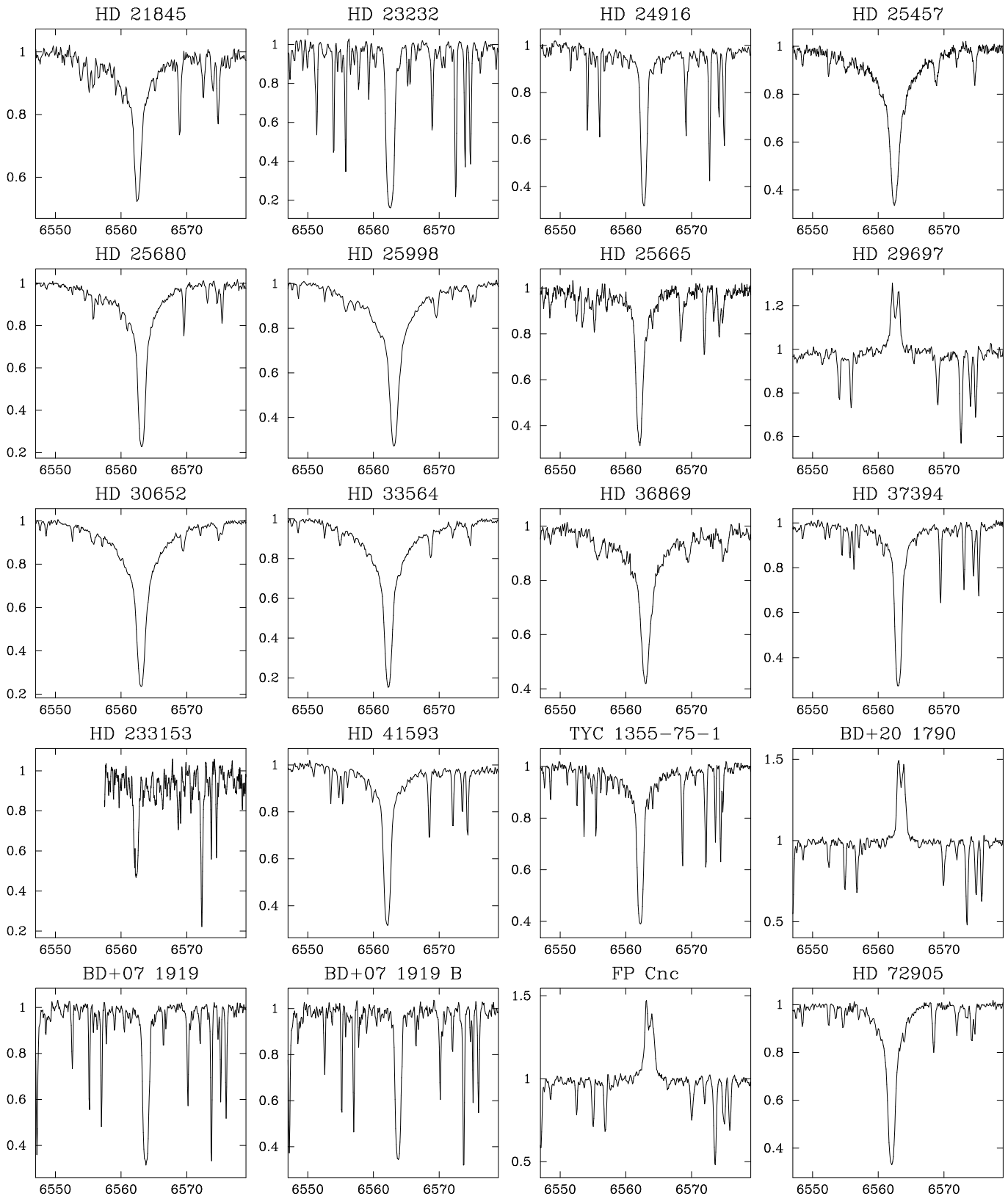


Fig. A.2. continued.

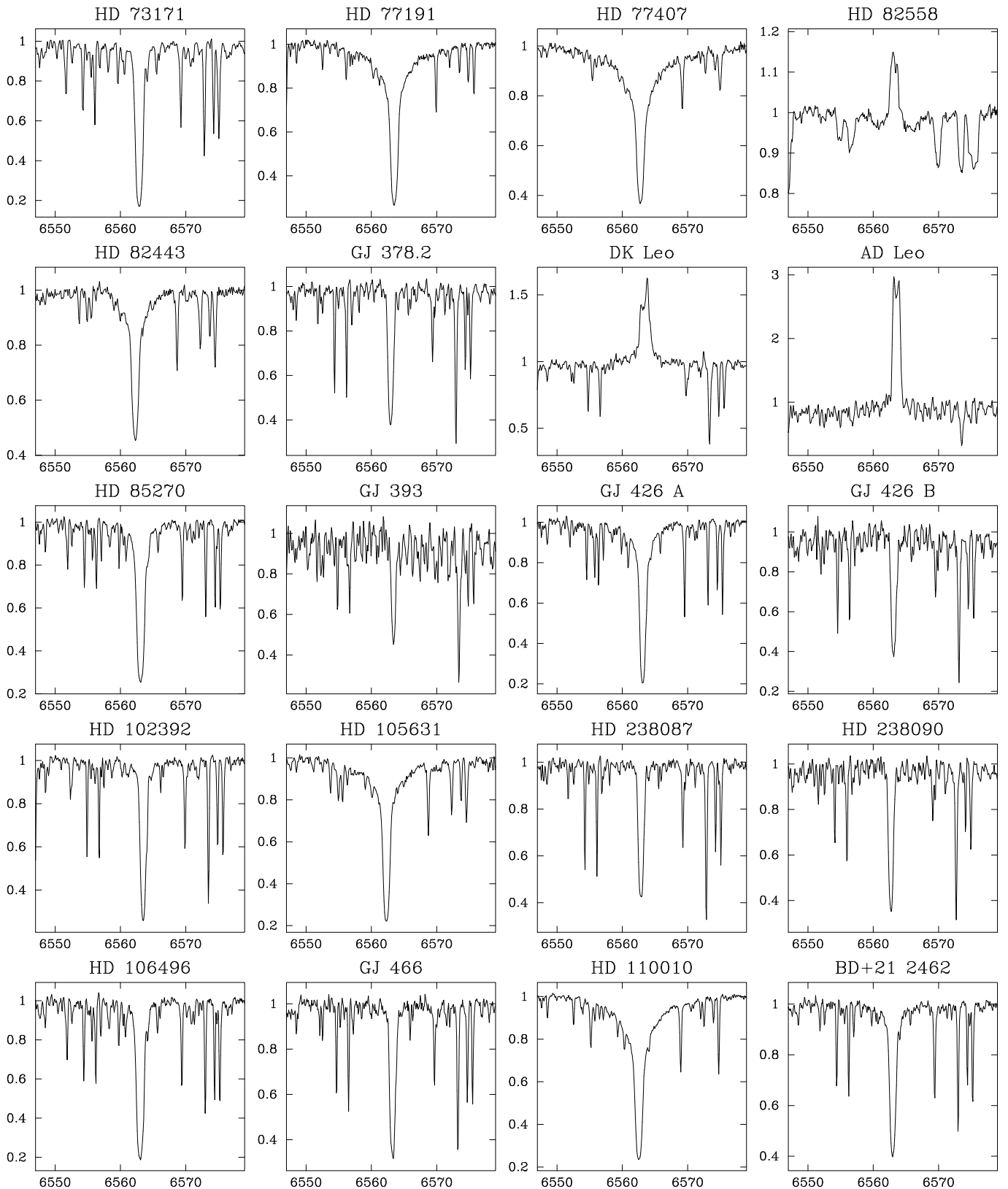


Fig. A.2. continued.

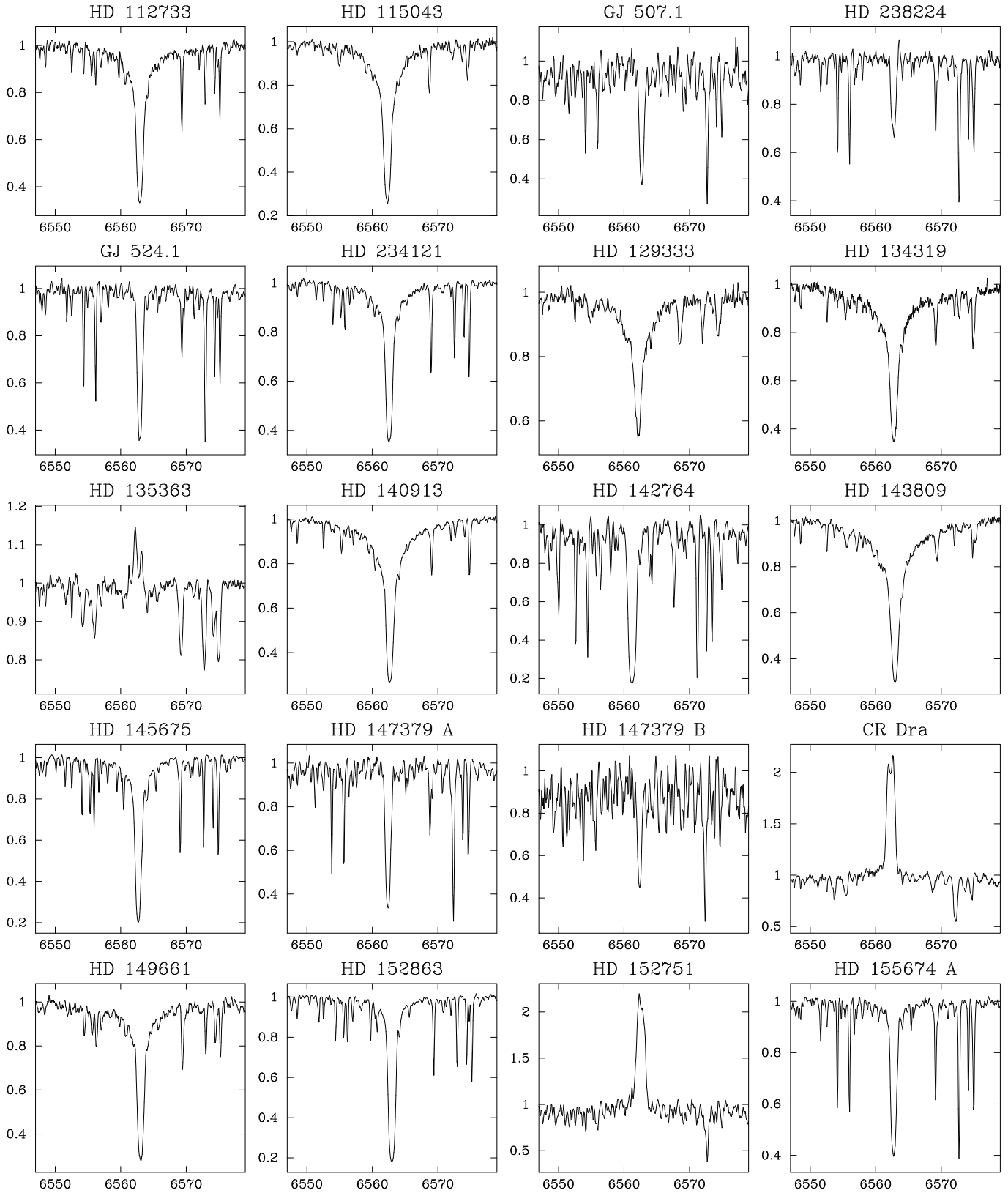


Fig. A.2. continued.

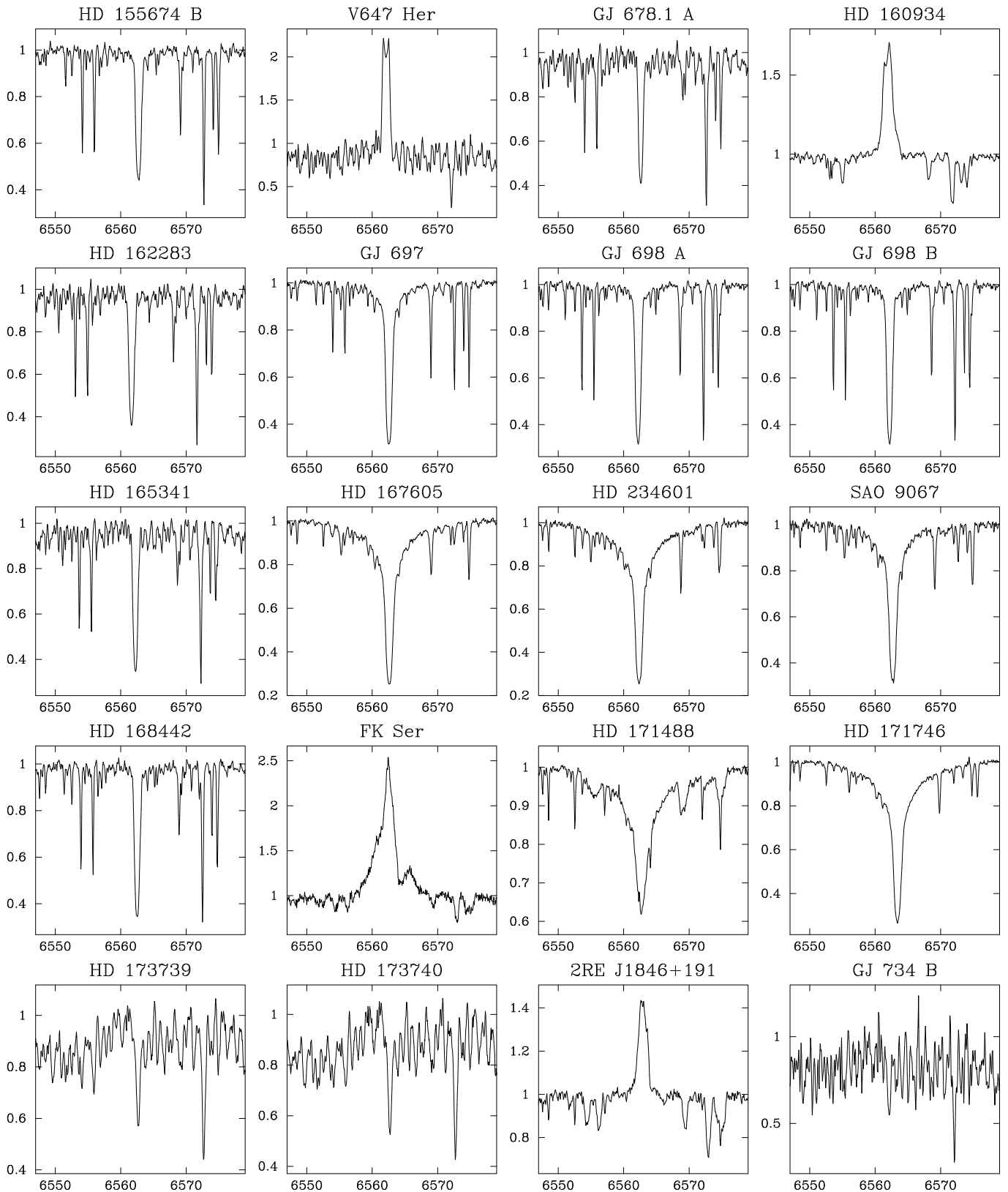


Fig. A.2. continued.

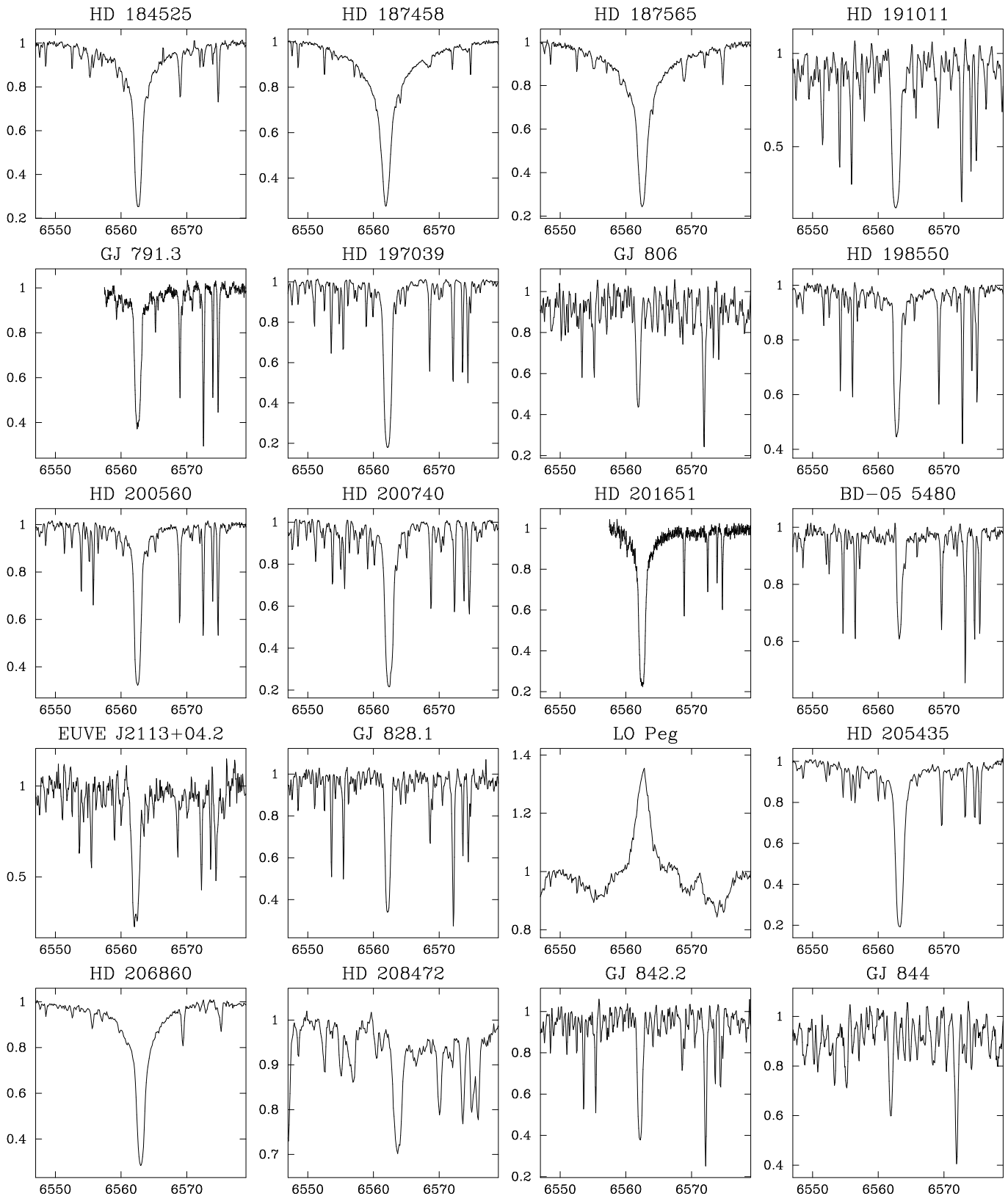


Fig. A.2. continued.

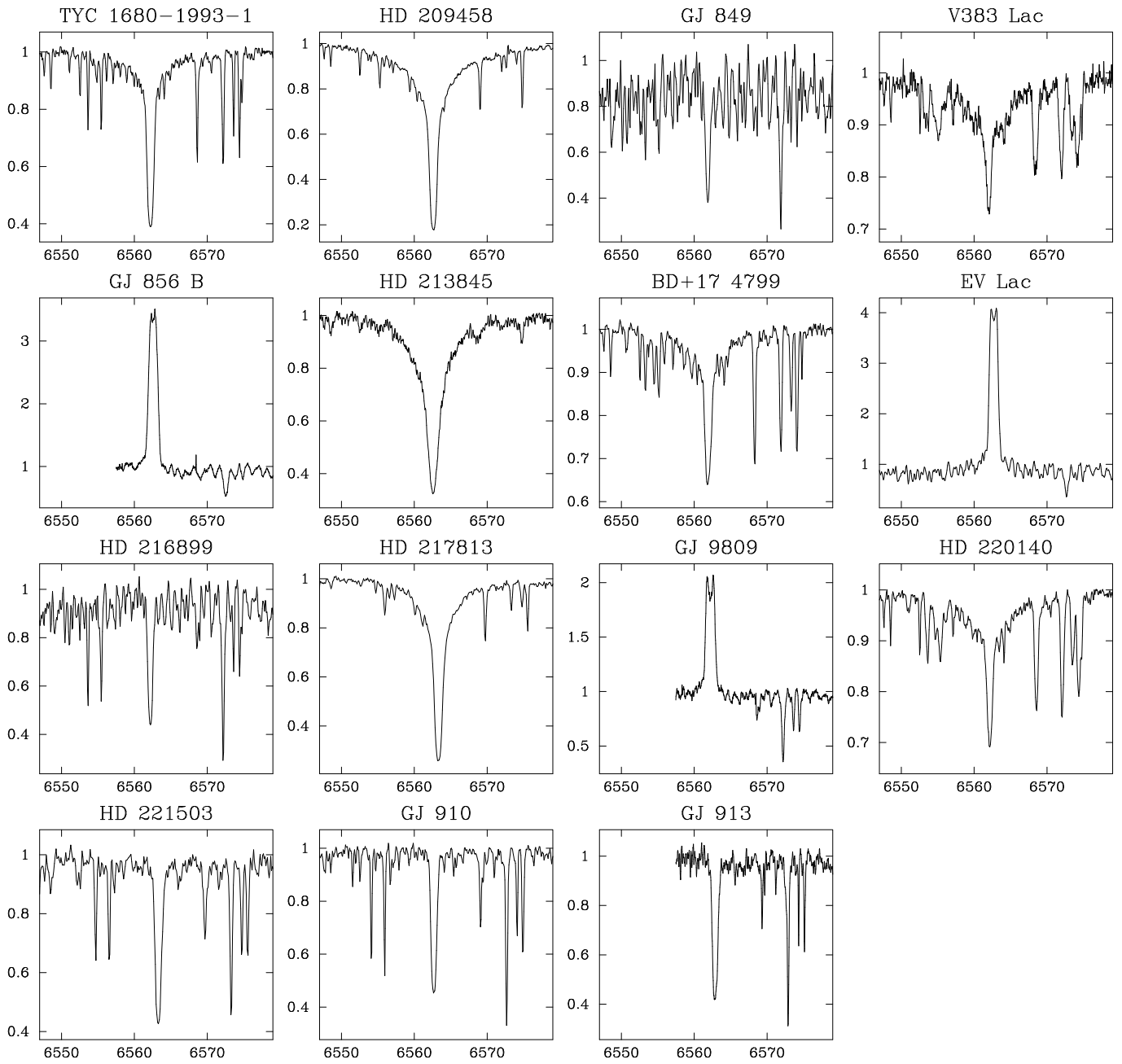


Fig. A.2. continued.

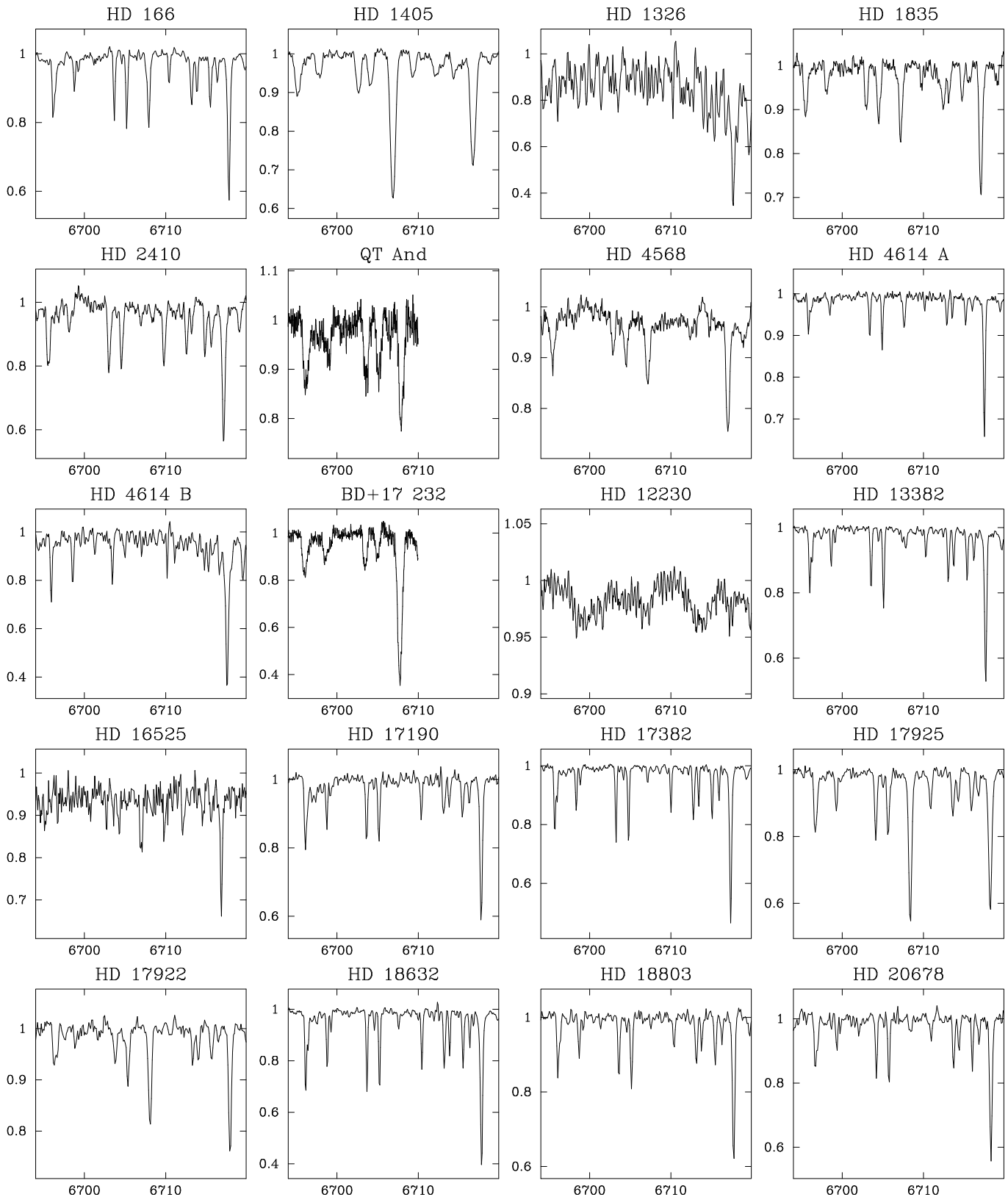


Fig. A.3. Li I spectra of the stars of our sample with observations of this line.

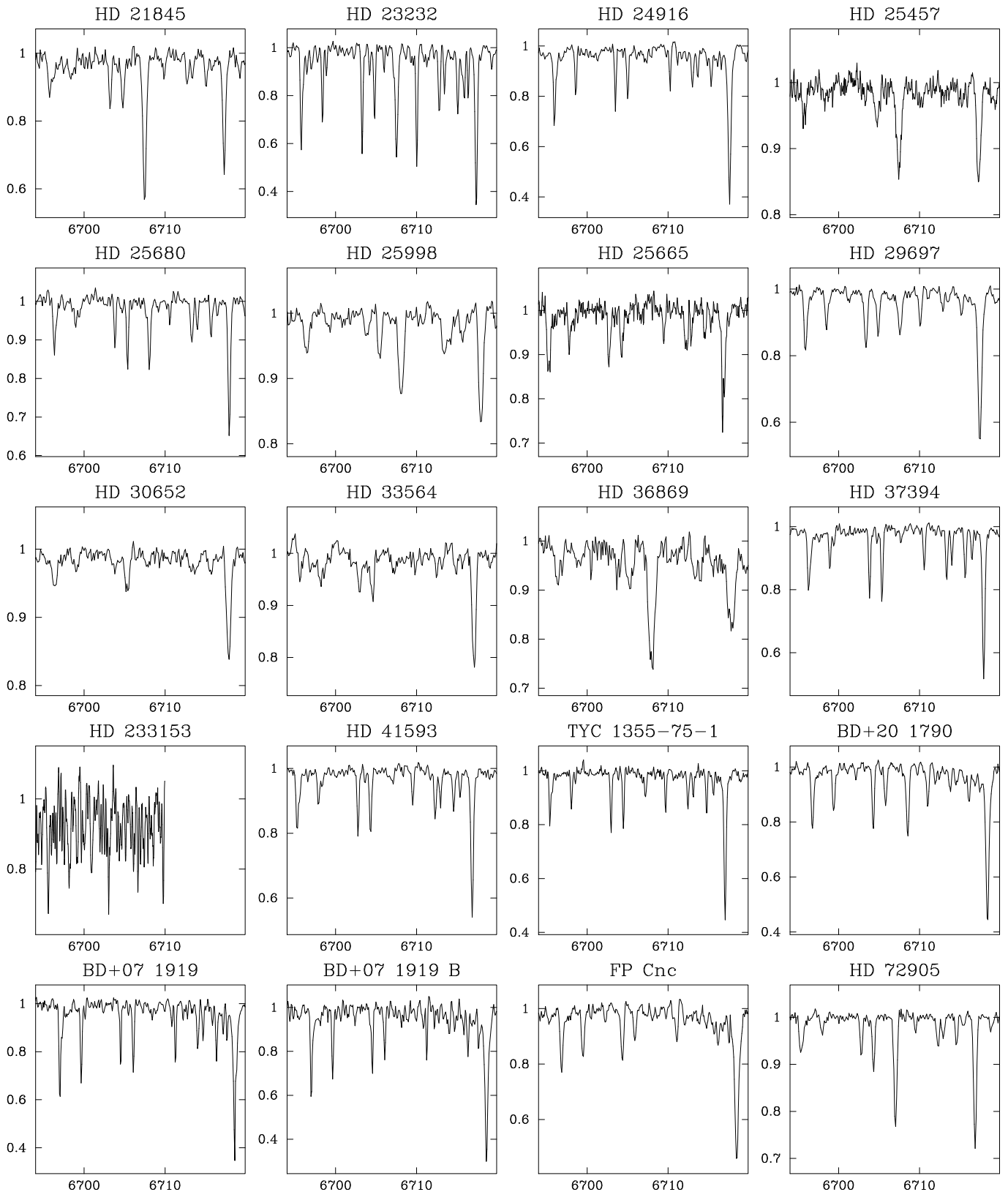


Fig. A.3. continued.

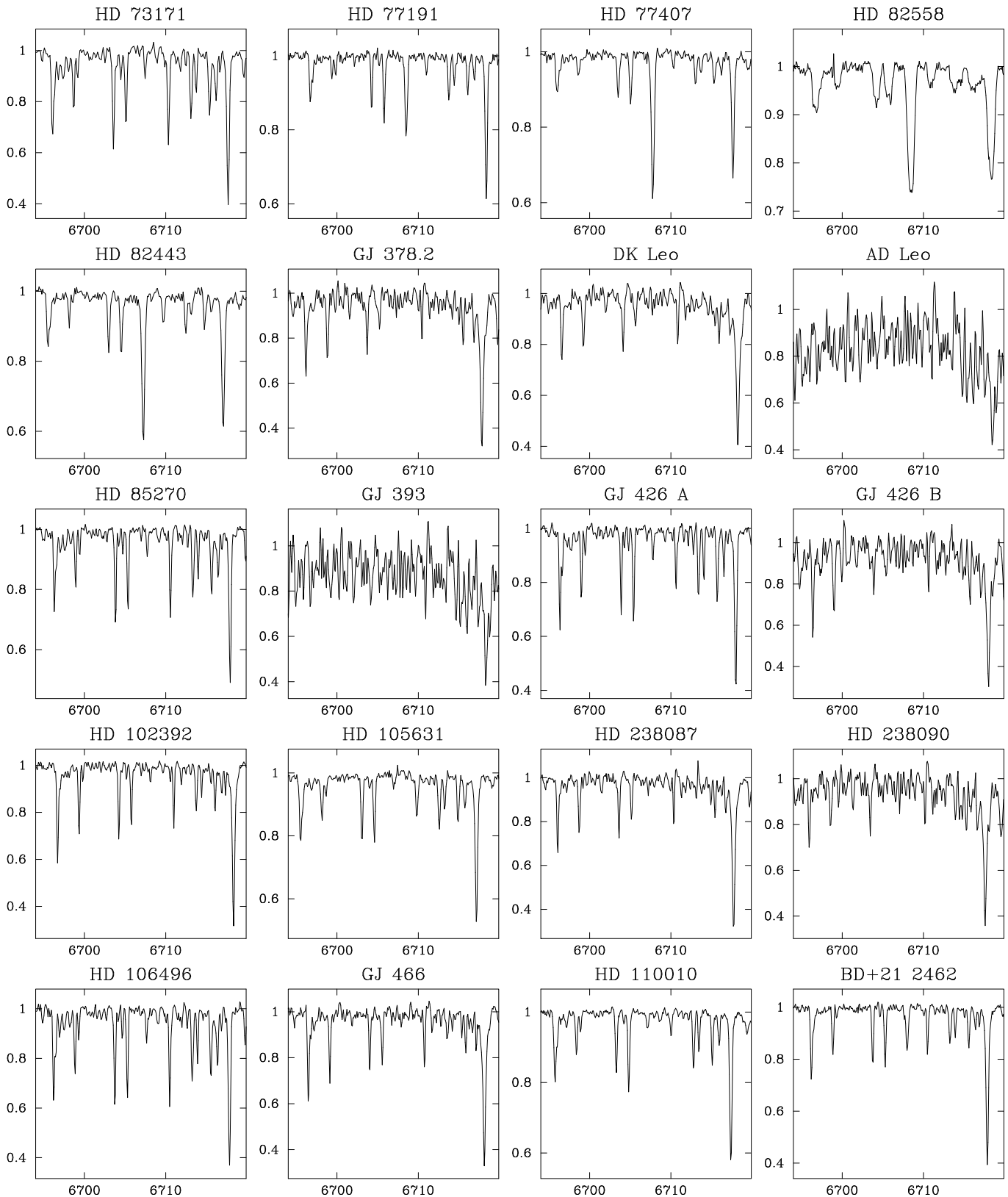


Fig. A.3. continued.

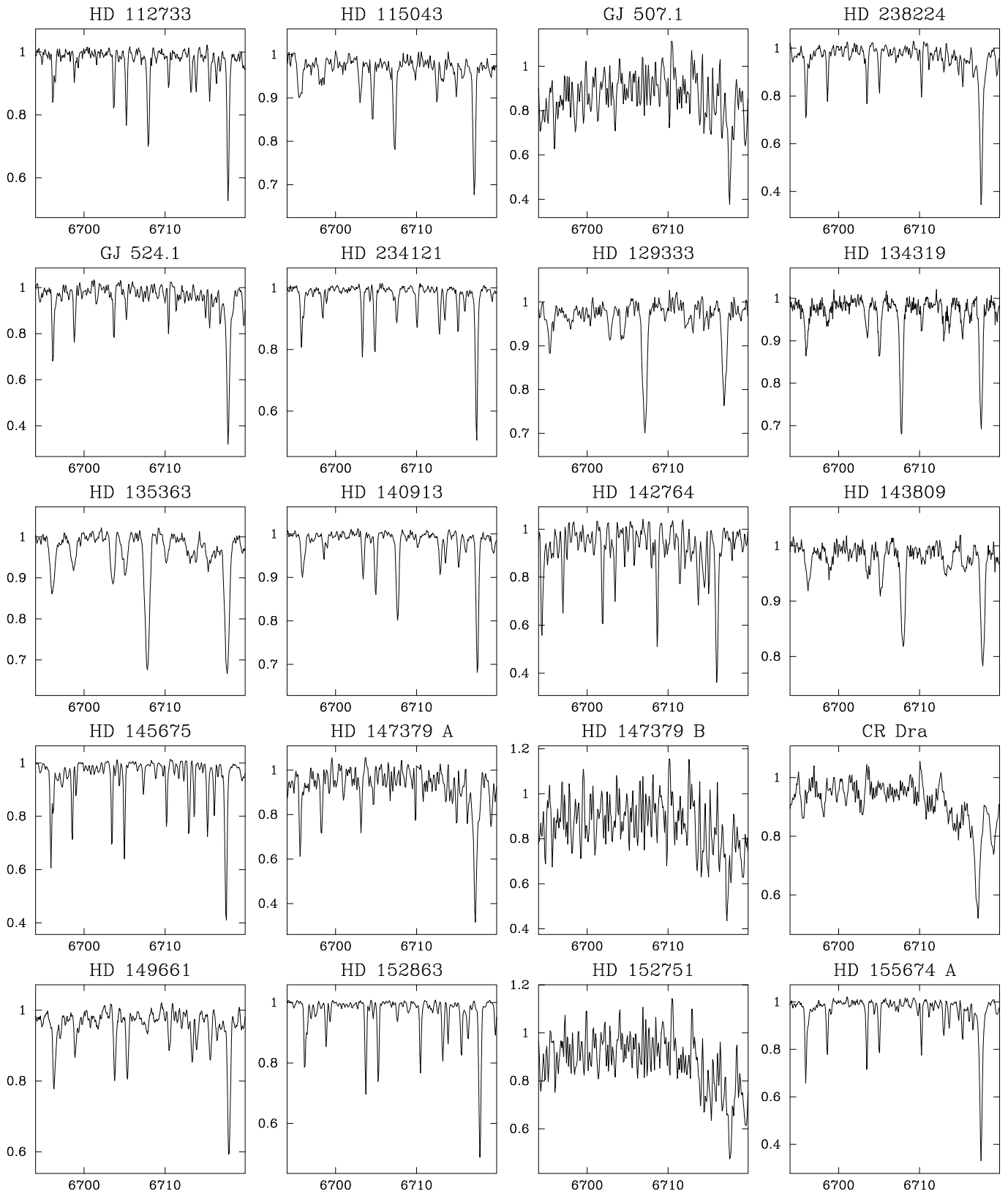


Fig. A.3. continued.

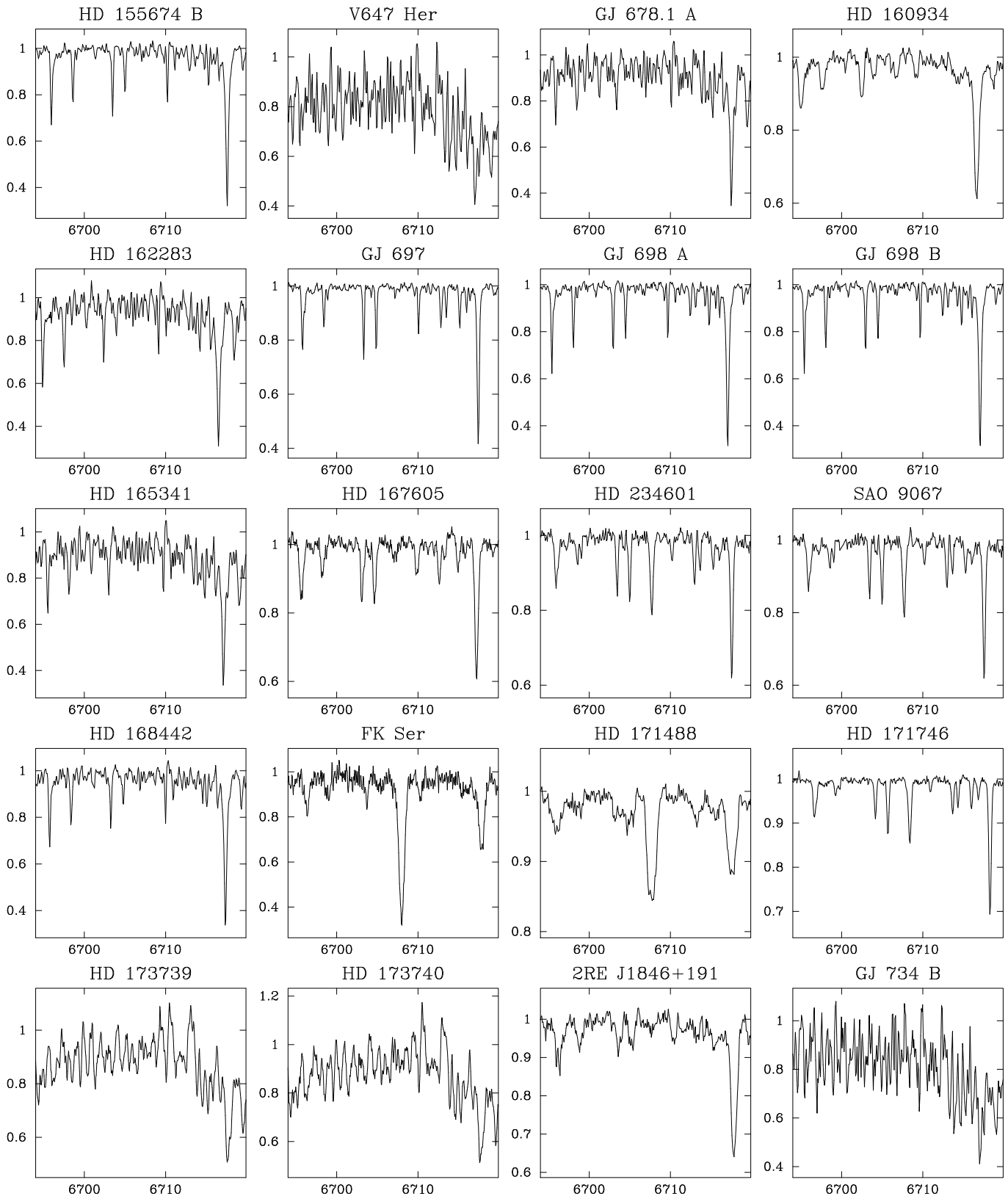


Fig. A.3. continued.

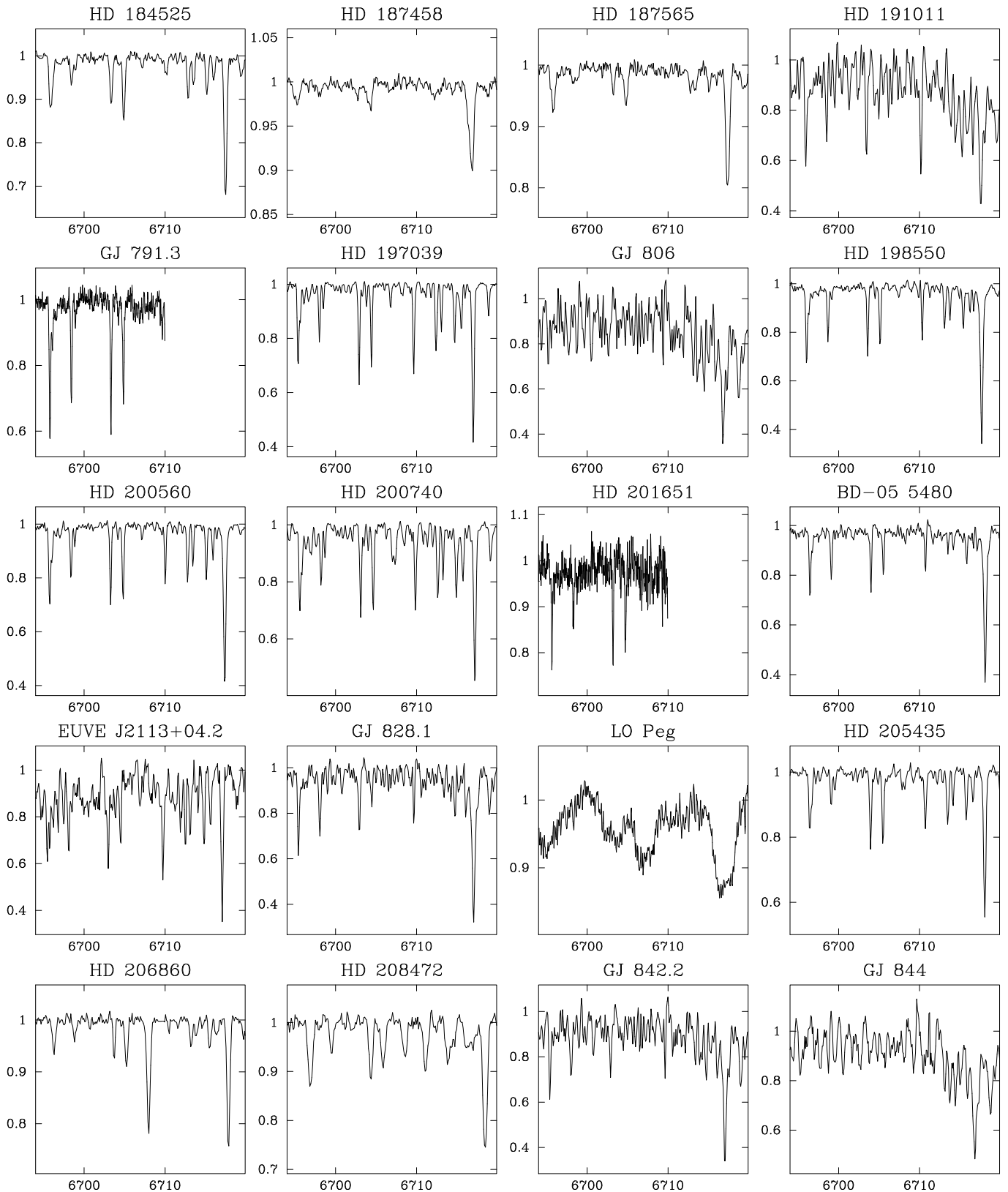


Fig. A.3. continued.

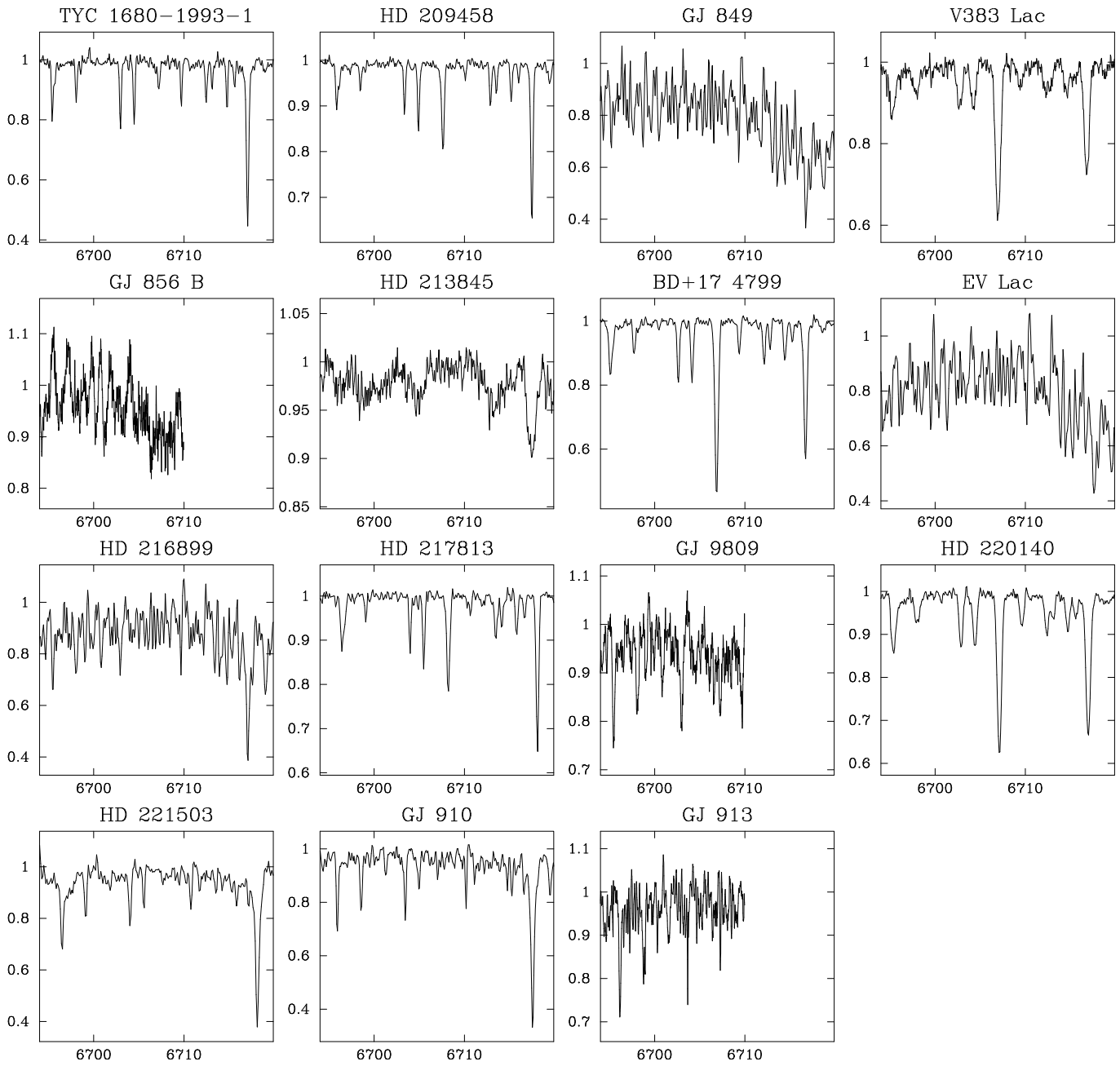


Fig. A.3. continued.

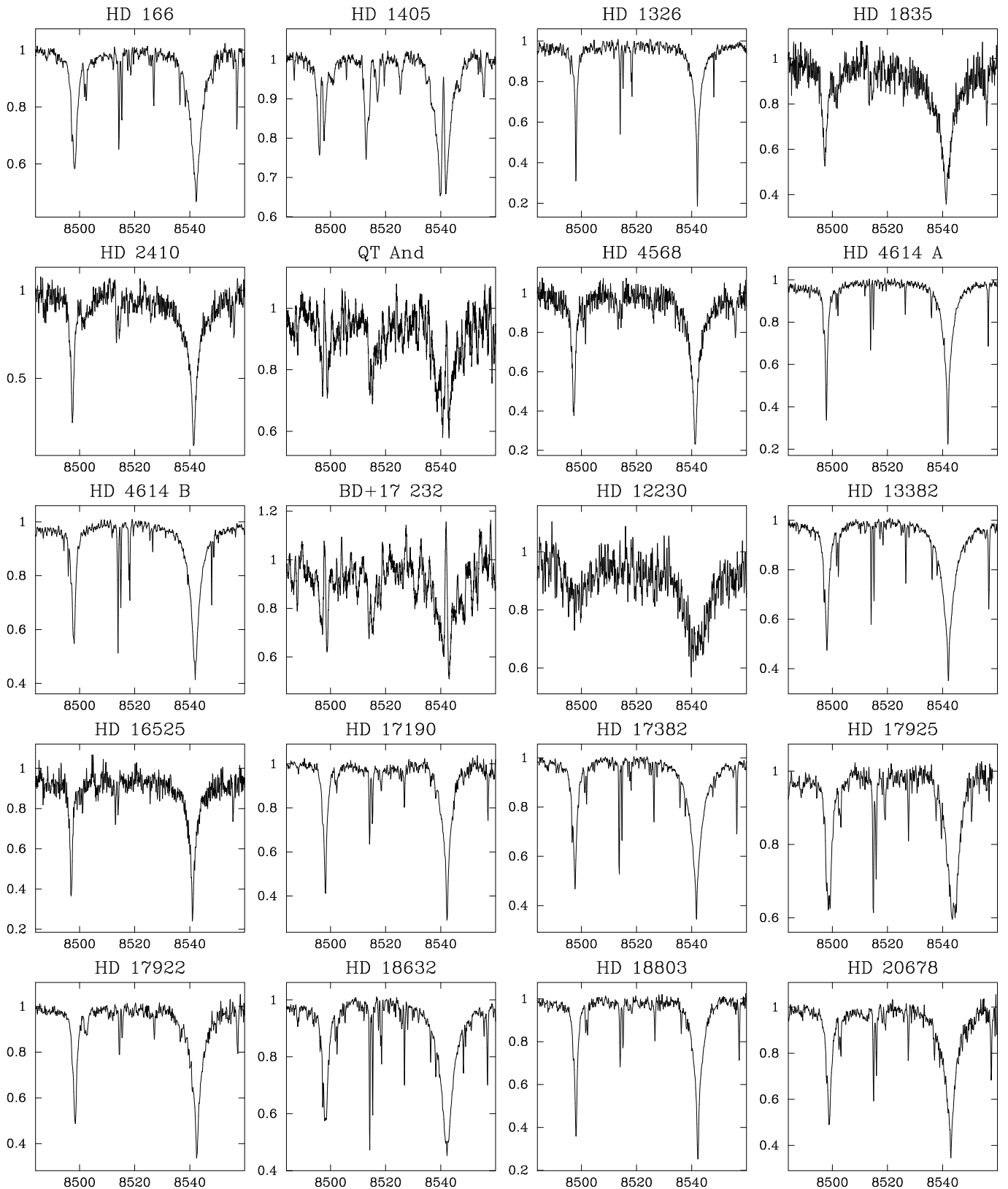


Fig. A.4. Ca II λ 8498 and 8540 Å spectra of the stars of our sample with observations of the Ca II infrared triplet.

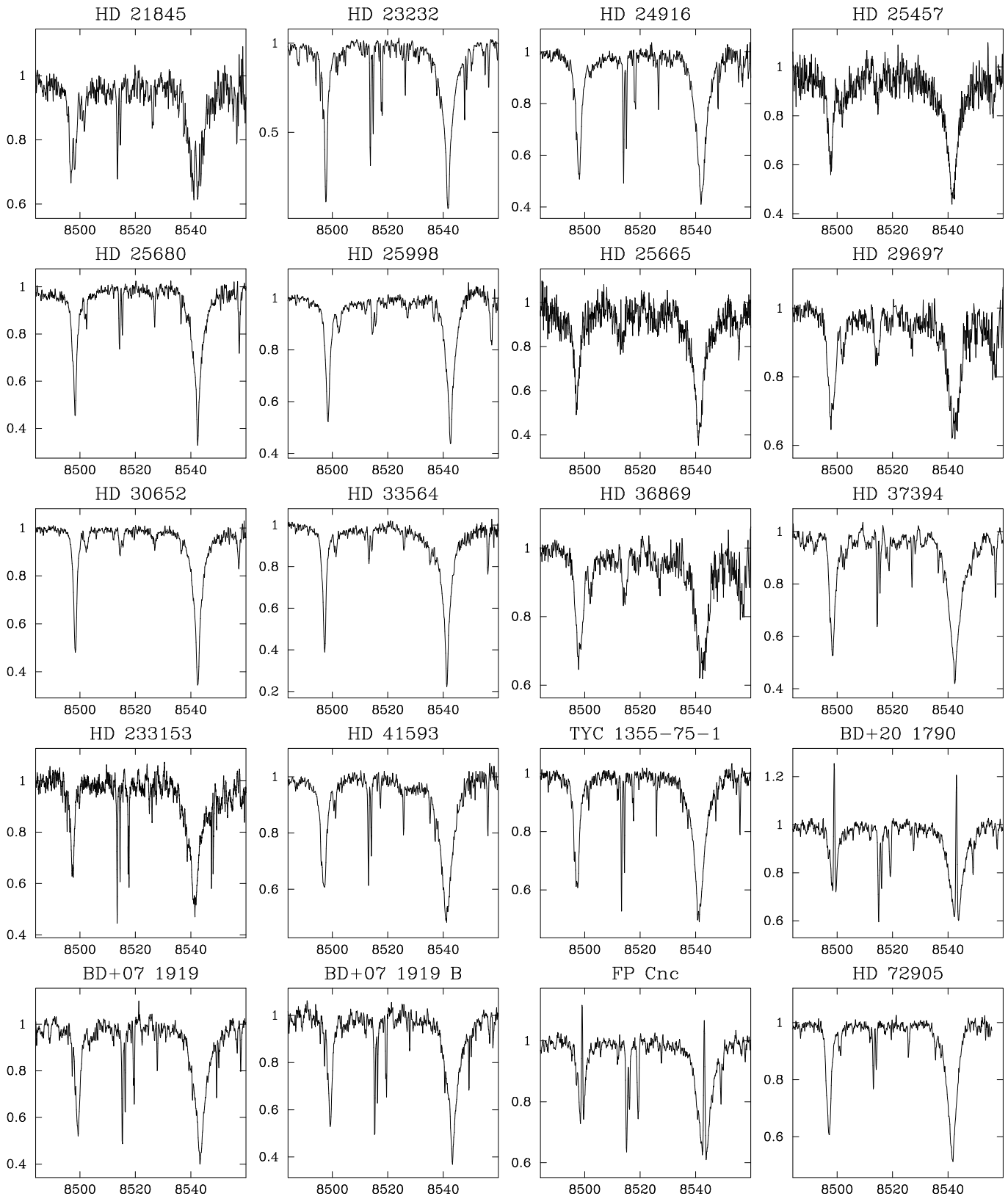


Fig. A.4. continued.

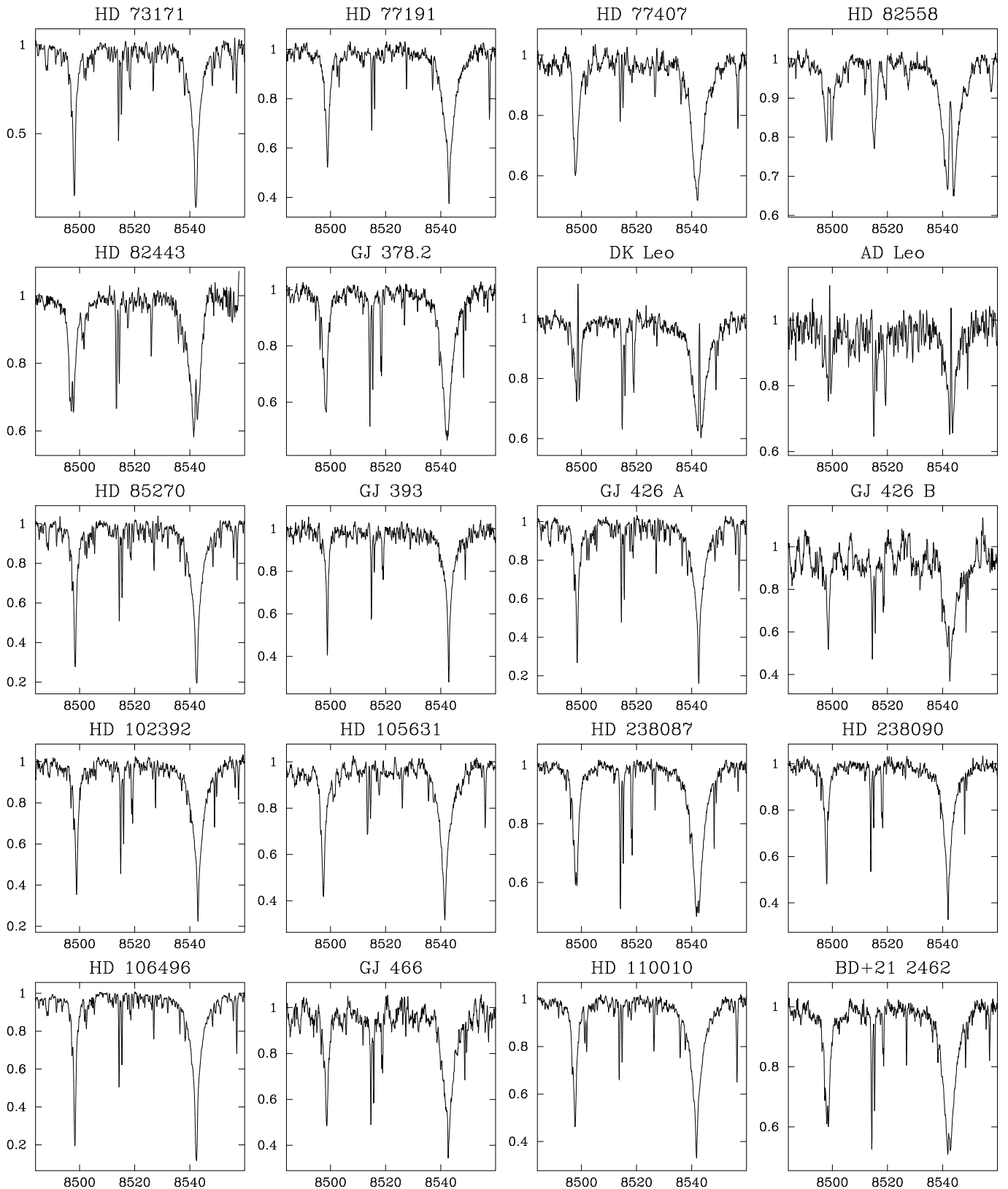


Fig. A.4. continued.

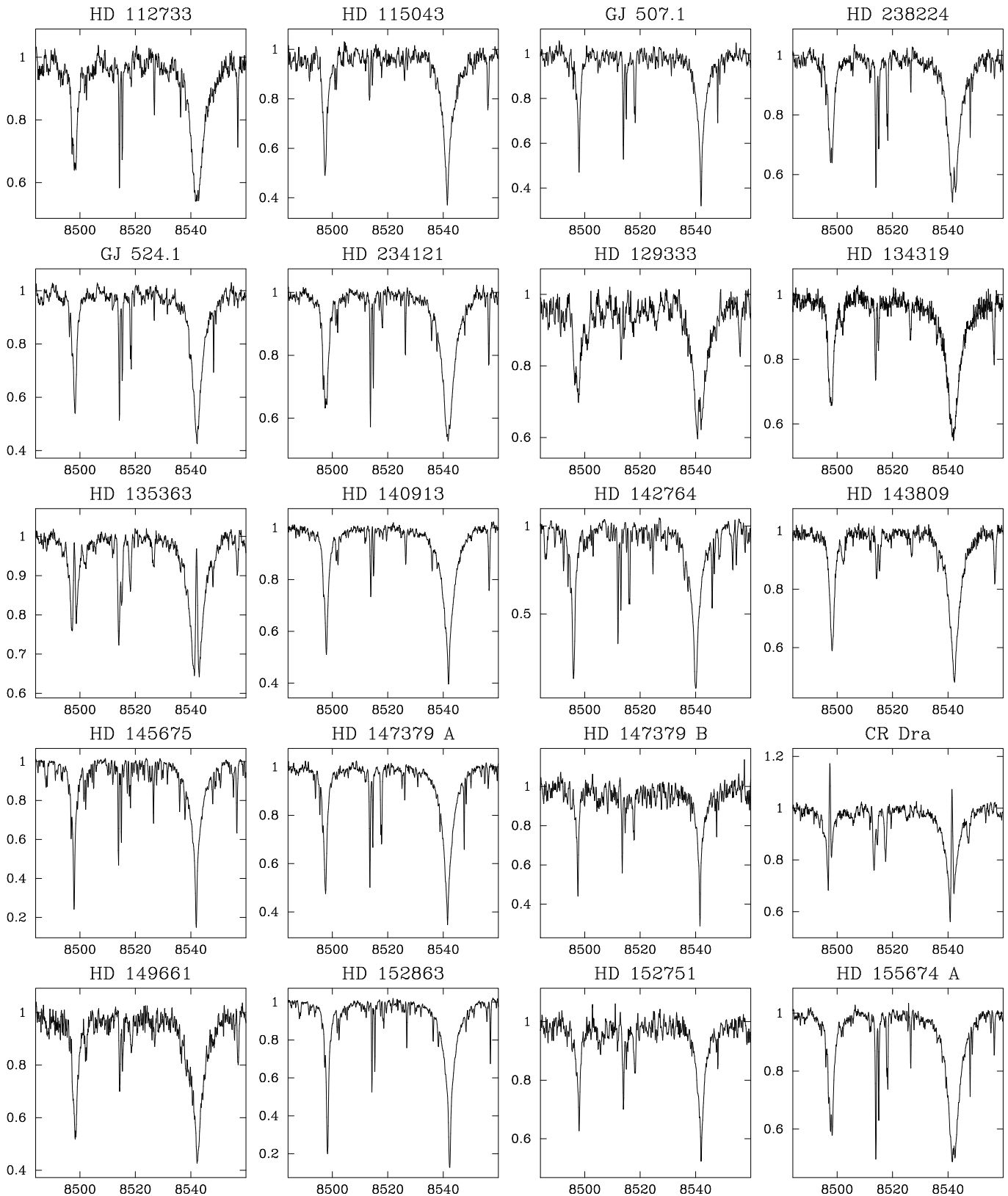


Fig. A.4. continued.

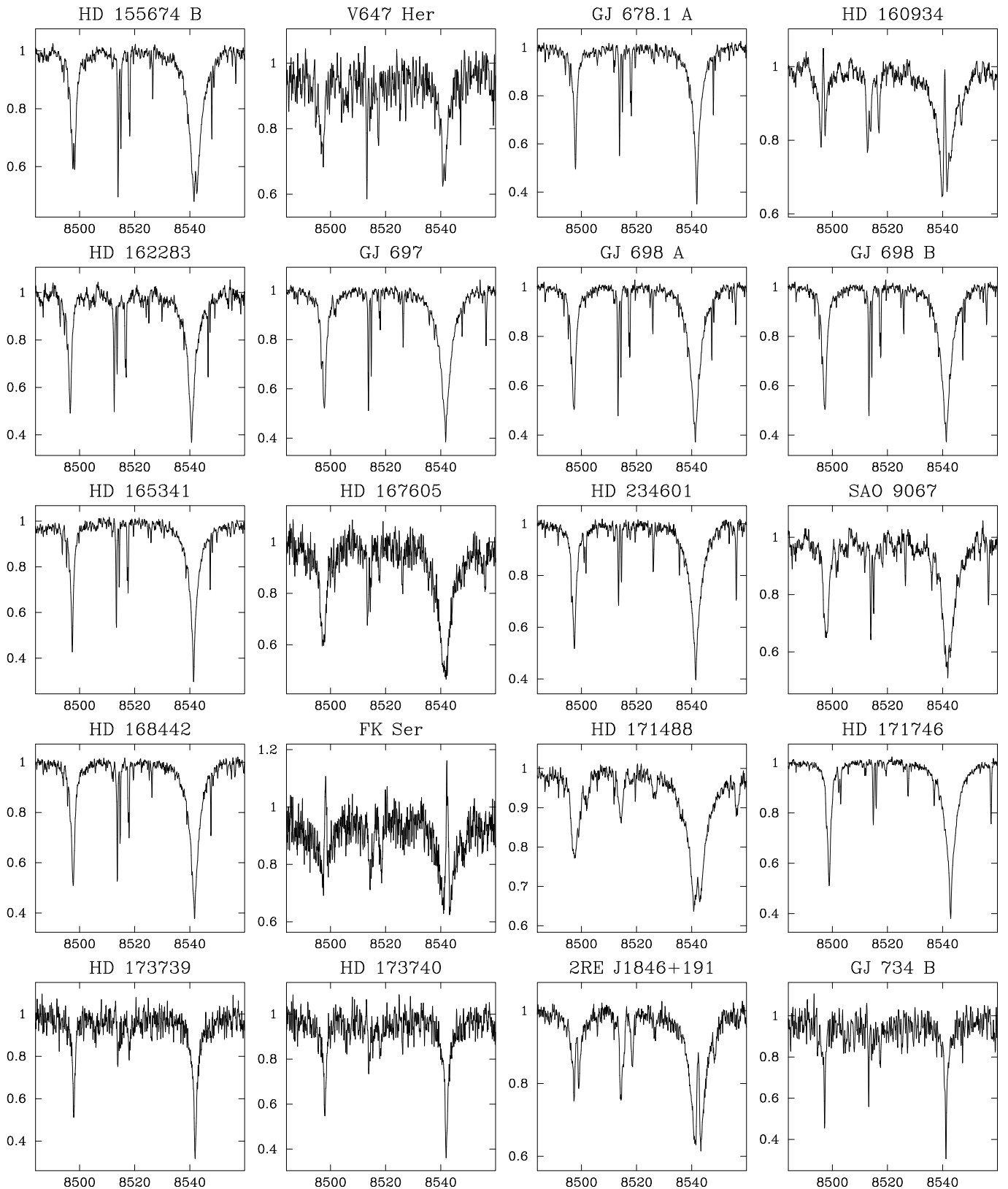


Fig. A.4. Continued.

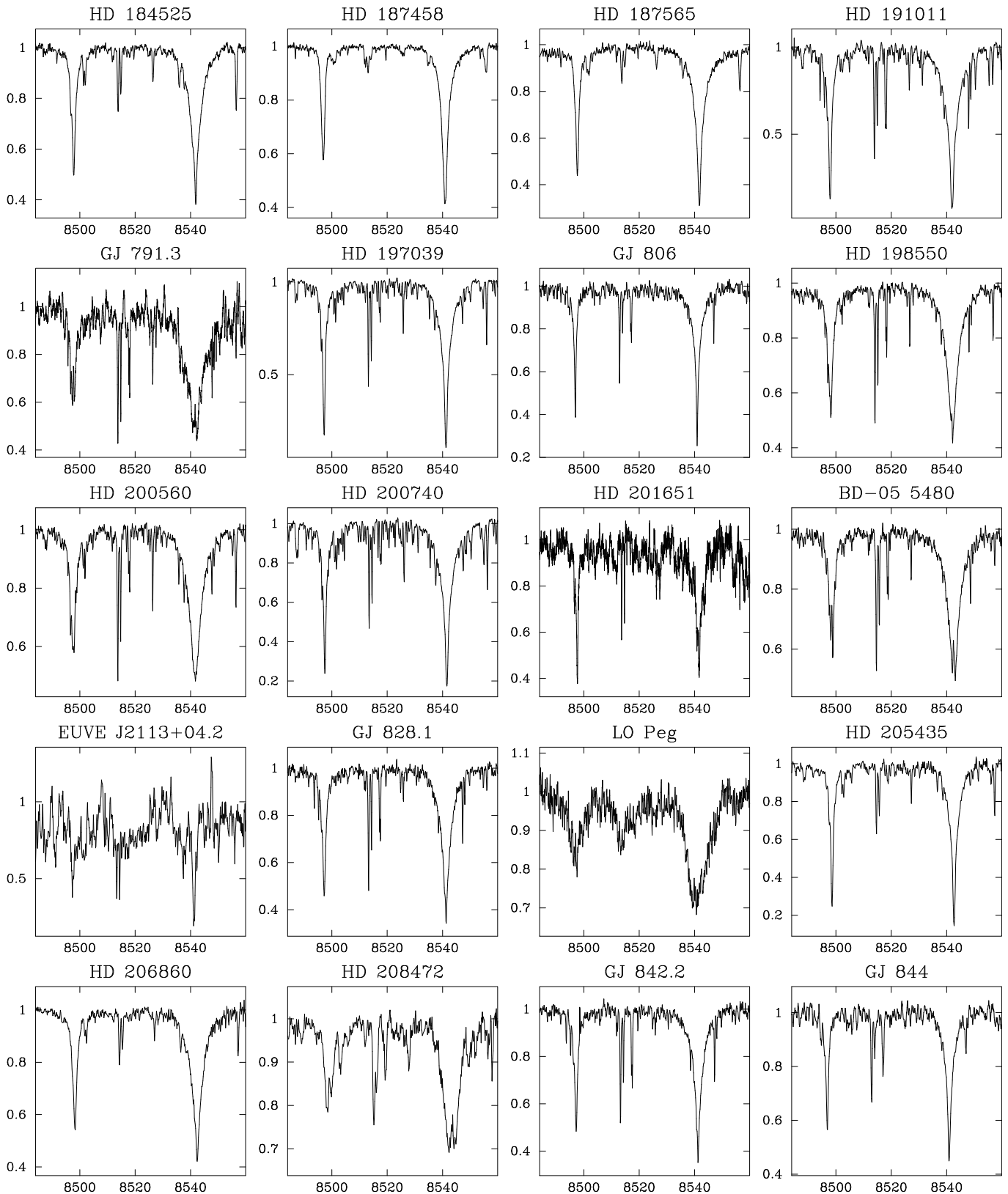


Fig. A.4. continued.

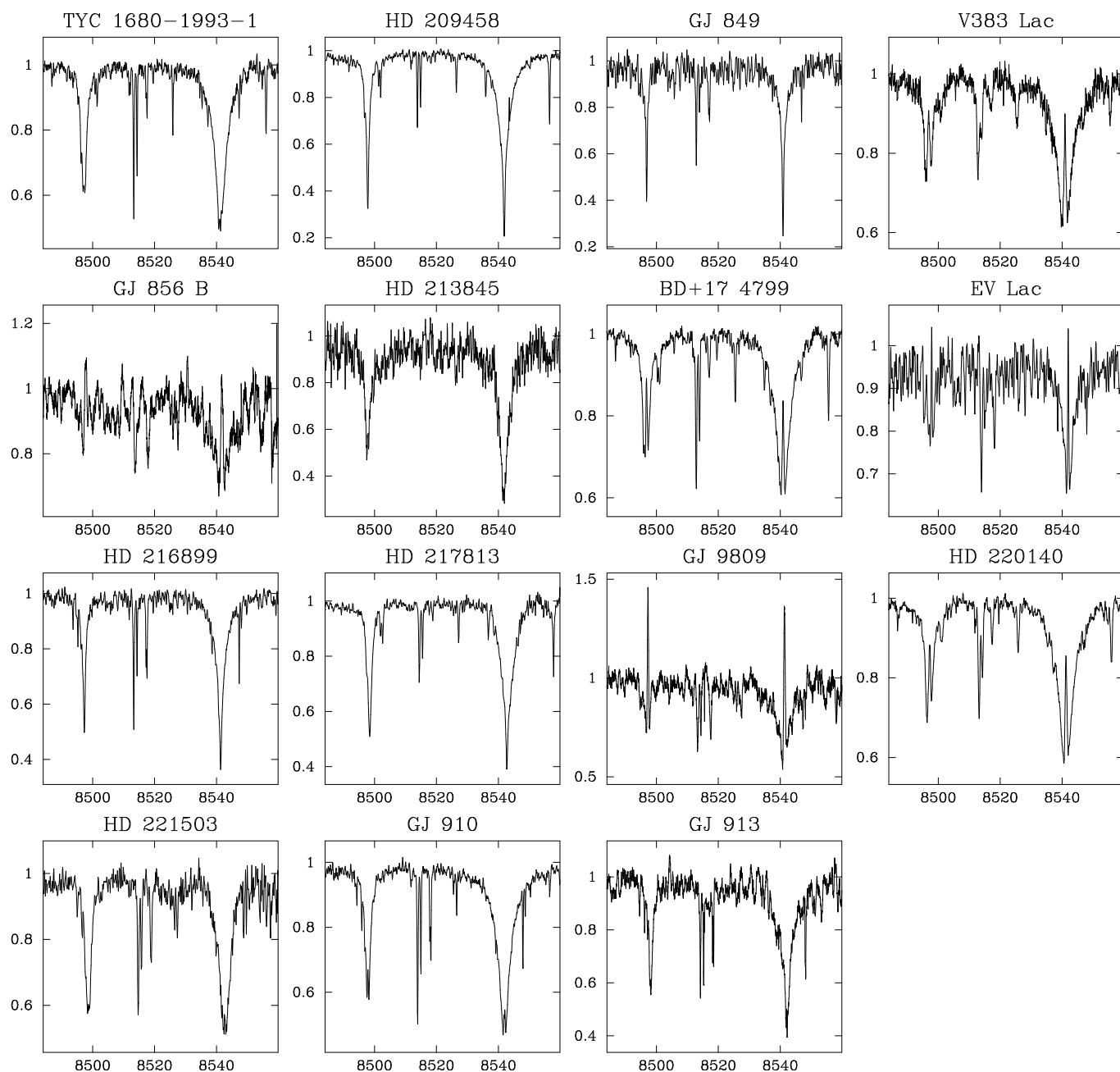


Fig. A.4. continued.